Exploring groundwater and soil water storage changes across the CONUS at 12.5 km resolution by a Bayesian integration of GRACE data into W3RA

Nooshin Mehrnegar[a], Owen Jones[b], Michael Bliss Singer[a,c,d], Maike Schumacher[e], Thomas Jagdhuber[f], Bridget. R. Scanlon[g], Ashraf Rateb[g], Ehsan Forootan[a,h]

[a] *School of Earth and Environmental Sciences, Cardiff University, CF103AT Cardiff, UK*
[b] *School of Mathematics, Cardiff University, CF244AG Cardiff, UK*
[c] *Water Research Institute, Cardiff University, CF103AX Cardiff, UK*
[d] *Earth Research Institute, University of California Santa Barbara, 91306 Santa Barbara, USA*
[e] *Institute of Physics and Meteorology (IPM), University of Hohenheim, 70593 Stuttgart, Germany*
[f] *Microwaves and Radar Institute, German Aerospace Center, 82234 Wessling, Germany*
[g] *Bureau of Economic Geology, Jackson School of Geosciences, University of Texas at Austin, TX 78758 Austin, USA*
[h] *Geodesy and Earth Observation Group, Institute of Planning, Aalborg University, Rendburggade 14, 9000 Aalborg, Denmark*

Abstract

Climate variability and change along with anthropogenic water use have affected the (re)distribution of water storage and fluxes across the Contiguous United States (CONUS). Available hydrological models, however, do not represent recent changes in the water cycle. Therefore, in this study, a novel Bayesian Markov Chain Monte Carlo-based Data Assimilation (MCMC-DA) approach is formulated to integrate Terrestrial Water Storage changes (TWSC) from the Gravity Recovery and Climate Experiment (GRACE) satellite mission into the W3RA water balance model. The benefit of this integration is its dynamic solution that uses GRACE TWSC to update W3RA's individual water storage estimates while rigorously accounting for uncertainties. It also downscales GRACE data and provides groundwater and soil water storage changes at ∼12.5 km resolution across the CONUS covering 2003-2017. Independent validations are performed against in-situ groundwater data (from USGS) and Climate Change Initiative (CCI) soil moisture products from the European Space Agency (ESA). Our results indicate that MCMC-DA introduces trends, which exist in GRACE TWSC, mostly to the groundwater storage and to a lesser extent to the soil water storage. Higher similarity is found between groundwater estimation of MCMC-DA and those of USGS in the southeastern CONUS. We also show a stronger linear trend in MCMC-DA soil water storage across the CONUS, compared to W3RA (changing from ±0.5 mm/yr to ±2 mm/yr), which is closer to independent estimates from the ESA CCI. MCMC-DA also improves the estimation of soil water storage in regions with high forest intensity, where ESA CCI and hydrological models have difficulties in capturing the soil-vegetation-atmosphere continuum. The representation of El Niño Southern Oscillation (ENSO)-related variability in groundwater and soil water storage are found to be considerably improved after integrating GRACE TWSC with W3RA. This new hybrid approach shows promise for understanding the links between climate and the water balance over broad regions.

Keywords:
CONUS; Markov Chain Monte Carlo (MCMC); GRACE TWSC; W3RA; Groundwater storage; Soil water storage;

1. Introduction

Reliable quantification of Terrestrial Water Storage Changes (TWSC, i.e., a vertical summation of canopy, surface water, snow, soil water and groundwater storage) and its spatiotemporal variability is required to understand numerous processes and feedback loops within the Earth's climate system. This quantification is also crucial for many applications related to hydrometeorology, water resources, hazard assessment, and land-atmosphere interactions, including flood and drought monitoring and prediction (*Houborg et al.*, 2012; *Long et al.*, 2013; *Slater et al.*, 2015; *Forootan et al.*, 2017, 2019; *Li et al.*, 2019), assessing water resources sustainability (*Scanlon et al.*, 2012a; *Forootan et al.*, 2014b; *Castellazzi et al.*, 2016), and identifying ecohydrological links between climate and vegetation (*Singer et al.*, 2014).

Over the past decades, climate variability and change along with anthropogenic modifications and land management activities have affected water resources across the Contiguous United States (CONUS) (*Fasullo et al.*, 2016; *Rodell et al.*, 2018). For example, increasing annual (net-)precipitation has resulted in several extreme drought and flood events across the country (*Schubert et al.*, 2004; *Dong et al.*, 2011; *Peterson et al.*, 2013; *Leng et al.*, 2016). In addition, the population has increased with an average annual growth of 0.67% between 2010 and 2019, mostly in the south and west parts, and the trend is expected to continue until 2050 (*Means III et al.*, 2005; *Potter and Hoque*, 2014). Groundwater across the CONUS accounts for almost half of the water consumed for irrigation, livestock, and drinking water (including public domestic water supply) (*Dieter*, 2018). In arid and semi-arid regions throughout much of the CONUS, groundwater is the only potential freshwater resource (*Maupin et al.*, 2017). As expected from the current hydro-climatological conditions, groundwater depletion has been reported in irrigated regions, such as the Central and Southern High Plains in Kansas and Texas and the Central Valley aquifers in California (*Famiglietti et al.*, 2011; *Scanlon et al.*, 2012a). Continuing the current negative trends in groundwater resources in these regions presents a dire threat to future crop production, natural stream-flow, groundwater-fed wetlands, salt water intrusion, and related ecosystems (*Scanlon et al.*, 2010).

Soil moisture is another key variable in the water cycle that can be used as a measure of the land-atmosphere feedback (*Levine et al.*, 2016). In general, soil moisture conditions contribute to the natural and agricultural productivity of a region by defining the vadose zone water that is available for uptake into vegetation (*Hillel*, 1998; *Illston et al.*, 2004). In turn, water is transpired from vegetation to the atmosphere during photosynthesis, increasing low-level atmospheric moisture at various scales. Therefore, information about soil moisture changes has been used to predict changes in precipitation (*Brocca et al.*, 2017), climatic extremes and future climate projections (*Bolten et al.*, 2009; *Mo et al.*, 2011). Soil moisture information is now used for monitoring and understanding drought development (see e.g., `www.drought.gov`). Satellite observations of time-variable gravity fields from the Gravity Recovery and Climate Experiment (GRACE, 2002–2017) satellite mission (*Tapley et al.*, 2004a,b) and its Follow-On mission (GRACE-FO, 2018–onward), provide an opportunity to estimate TWSC globally with a spatial resolution of a few 100 km and temporal resolution of ∼10 days to 1 month (*Flechtner et al.*, 2016). The ability of GRACE satellites to detect water storage changes in the sub-surface and its sensitivity to water stresses throughout all seasons provides a unique opportunity to extract possible intensification's of the water cycle (*Eicker et al.*, 2016; *Kusche et al.*, 2016) and for drought monitoring at global (*Zhao et al.*, 2017b; *Forootan et al.*, 2019) and regional scales (*Houborg et al.*, 2012; *Thomas et al.*, 2014; *Zhao et al.*, 2017a; *Sinha et al.*, 2017; *Schumacher et al.*, 2018). In recent years, various studies indicate that by integrating GRACE TWSC into hydrological models, one can spatially downscale and vertically dis-aggregate GRACE TWSC

into its individual surface and sub-surface water storage estimates. The integration of remote sensing data and models lends more realism to such water storage estimates. To achieve this goal, these studies have applied data-model fusion techniques such as sequential ensemble Kalman filter and Smoother or their extensions (see e.g., *Zaitchik et al.*, 2008; *Van Dijk et al.*, 2014; *Girotto et al.*, 2016, 2017; *Schumacher et al.*, 2016, 2018; *Khaki et al.*, 2017), statistical inversion (*Forootan et al.*, 2014c, 2017), deep learning (*Miro and Famiglietti*, 2018) and Bayesian state-space method (*Mehrnegar et al.*, 2020). Integration of GRACE data into Land Surface Models (LSMs, *Zaitchik et al.*, 2008) is also done in the United States (US) drought monitoring system [1], which produces groundwater and soil moisture drought indicators, and predictions of groundwater changes.

The objective of this study is to explore meso-scale soil water storage and groundwater storage changes across the CONUS, with an emphasis on the use of a relatively simple water balance model. Therefore, the Worldwide Water Resources Assessment (W3RA, *Van Dijk*, 2010) model, that is simpler than the currently used NASA's Catchment Land Surface Model (CLSM, *Ducharne et al.*, 2000), is selected as our platform, which is adapted here by defining the CONUS boundary as its domain covering the period 2003-2017. The ERA-Interim's interpolated forcing data (*Dee et al.*, 2011) are used as model input with the spatial resolution of $\sim$12.5 km.

A novel Bayesian approach is formulated in this study which uses GRACE TWSC to update an ensemble of monthly averaged W3RA water storage simulations. The mathematical formulation is an extension of the Dynamic Model Data Averaging (DMDA) introduced by *Mehrnegar et al.* (2020). The new formulation consists of a combination of a forward-filtering backward-smoothing recursion approach (*Kitagawa*, 1987) and a Markov Chain Monte Carlo (MCMC, *Geyer*, 1991) algorithm. This method, which is referred here to as 'MCMC-Data Assimilation (MCMC-DA)', can be used to recursively estimate unknown state parameters (individual surface and sub-surface water storage), as well as temporal dependency between them, which are allowed to vary over time. The difference between MCMC-DA and DMDA (*Mehrnegar et al.*, 2020) is that DMDA estimates the unknown state parameters using a Kalman Filtering (KF, *Kalman*, 1960) approach, while the temporal dependency between the unknown individual water storage states is controlled by a constant forgetting factor ranging from 0 to 1. The computation of this constant value can only be done empirically, and therefore, it is considered as a source of increasing uncertainties in the DMDA individual water storage estimations. A physical explanation of this problem is the fact that the magnitude of changes in water storage components depends on the history of hydrological processes. However, there is little physical knowledge about how this dependency varies over time. Therefore, selecting a constant forgetting factor cannot be physically justified, though, the value could be mathematically optimized to provide an overall best fit between the model's unknown states and GRACE TWSC as was achieved by *Mehrnegar et al.* (2020). To eliminate this drawback, here, an MCMC process replaces the constant forgetting factor to allow dynamic estimation of temporal dependencies among unknown state parameters (i.e., individual water storage in various compartments). As a result, more realistic estimates of individual water storage components can be expected from the introduced MCMC-DA. We show that by formulating the rigorous Bayesian data-model integration, GRACE TWSC improves model estimates of both soil water storage and groundwater storage changes in terms of trends and seasonality, which are not well simulated by most of available models (*Scanlon et al.*, 2019). Beyond long-term trends and seasonality, climate cycles, such as El Niño Southern Oscillation (ENSO, *Barnston and Livezey*, 1987), a dominant climate mode that results from

[1] https://grace.jpl.nasa.gov/applications/drought-monitoring/

ocean–atmosphere interactions over the equatorial Pacific (*Trenberth and Stepaniak*, 2001), considerably influence precipitation and inter-annual TWSC in various regions (*Chen et al.*, 2010; *Fasullo et al.*, 2013; *Awange et al.*, 2014; *Zhang et al.*, 2015; *Forootan et al.*, 2016; *Ni et al.*, 2018; *Anyah et al.*, 2018; *Forootan et al.*, 2019). Previous studies explored the influence of ENSO on GRACE TWSC and the global water balance estimates (*Phillips et al.*, 2012; *Eicker et al.*, 2016; *Forootan et al.*, 2018). Their results indicate that the ENSO teleconnection patterns are well reflected in the GRACE signal, whereas more pronounced variability is found by GRACE than the reanalysis water flux estimates shown by *Eicker et al.* (2016). Therefore, in this study, we examine how combining GRACE and W3RA changes the ENSO-related variability in groundwater and soil water storage estimates across the CONUS .

In what follows, the W3RA model and data sets used in this study are described in Section 2, and the proposed MCMC-DA is formulated in Section 3. In Section 4, the MCMC-DA groundwater and soil water storage estimates are compared with those of the original model outputs, while the possible relationships between the storage changes and climatic and anthropogenic factors are evaluated. Validations are done against independent measurements, i.e., in-situ USGS groundwater level observations, as well as soil moisture data from the European Space Agency (ESA)'s Climate Change Initiative (CCI). Evaluations using the groundwater levels are done after standardizing available time series. Within Texas and California, where reliable information is available, the equivalent groundwater storage estimates are computed from the USGS level observations, then, these values are used to evaluate groundwater storage estimates from MCMC-DA and the original model within these states.

To extract the influence of ENSO on groundwater and soil water storage estimates, the Independent Component Analysis (ICA, *Forootan and Kusche*, 2012, 2013; *Forootan et al.*, 2018) is applied, and the results are compared with available ENSO indices and interpreted in Section 4. Changes in groundwater and soil water storage within the Texas and California states, which are mostly affected by anthropogenic modifications, are evaluated and interpreted in Section 4. Finally in Section 5, the main conclusions and an outlook are provided. This study contains an Electronic Supporting Material (ESM) that provides the details of MCMC-DA, and auxiliary information to better understand the performed investigations.

2. Data and model

2.1. W3RA water balance model

The W3RA water balance model was first developed in 2008 by the Commonwealth Scientific and Industrial Research Organization (CSIRO). W3RA is a grid-distributed water balance model that simulates landscape water storage in the vegetation and soil systems at a $1^\circ \times 1^\circ$ resolution (*Van Dijk*, 2010). We modified the original code [2] for the CONUS by improving the spatial resolution to $0.125^\circ \times 0.125^\circ$. The model simulates the grid-based water balance, including surface water storage, surface soil layer (top layer), shallow rooted, and deep rooted soil layers, and groundwater storage. In W3RA, each cell is modeled independently of its neighbors but lateral mass exchanges are accounted for by implementing a routing scheme. More details on the W3RA model can be found in *Van Dijk* (2010).

Daily $0.125^\circ \times 0.125^\circ$ interpolated ERA-Interim reanalysis fields (*Dee et al.*, 2011) of precipitation, albedo, 2-meter wind, as well as minimum and maximum temperature [3] are used

[2] http://wald.anu.edu.au/challenges/water/w3-and-ozwald-hydrology-models/
[3] https://apps.ecmwf.int/datasets

as forcing to run the model from 1980-2017. In this study, we use W3RA's monthly averaged model states (surface water storage+ surface soil water (top layer) + shallow rooted soil water + deep rooted soil water storage + groundwater storage= TWSC), which are known as the W3RA's water storage components throughout this paper, for the period January 2003 through December 2017. Model uncertainty is estimated following *Renzullo et al.* (2014) by using the perturbed meteorological forcing approach. To this end, we assume an additive error for the shortwave radiation perturbation of 50 Wm^2, a Gaussian multiplicative error of 30% for rainfall perturbation, and a Gaussian additive error of 2 °C as the magnitude of the additive error air temperature perturbations. Estimated model uncertainty is used subsequently as the initial value of the variance/covariance matrix of the unknown state parameter (see ESM- Section 1.2.1) in the Bayesian inference, which is then updated through a forward-filtering and backward smoothing algorithm presented in ESM- Section 1.2.2.

2.2. GRACE TWSC

In this study, we use the latest release (RL06) monthly GRACE level 2 (L2) product, provided by the Center for Space Research (CSR [4]) for January 2003 through December 2017. The potential coefficients are truncated at the spherical harmonics of degree and order 90, resulting in ∼300 km spatial resolution at the Equator. In order to generate monthly TWSC fields from GRACE products, recommended corrections are applied to the GRACE spherical harmonic coefficients. To this aim, degree 1 coefficients, which are not observed by GRACE, are replaced by those from *Swenson et al.* (2008) to account for the movement of the mass center of the Earth. Degree 2 and order 0 (C_{20}) coefficients are replaced by more reliable estimates of the Satellite Laser Ranging (SLR) solutions following *Chen et al.* (2007). Surface deformation signals due to the Glacial Isostatic Adjustment (GIA) are reduced using *Wahr and Zhong* (2012)'s model.

Correlated errors of the potential coefficients, which are caused by anisotropic spatial sampling of the mission, instrument noise, and temporal aliasing from incomplete reduction of short-term mass variations (*Forootan et al.*, 2014a), are reduced by applying the DDK2 filter (*Kusche et al.*, 2009). The formulation in *Wahr et al.* (1998) is used to convert the L2 potential coefficients to $0.125° \times 0.125°$ girdded TWSC for the CONUS, while covering the period of 2003-2017. Signal attenuation in GRACE TWSC fields is accounted for by grid-based scales derived by dividing the original W3RA TWSC fields and those smoothed by the DDK2 filter (similar to *Landerer and Swenson*, 2012). Uncertainties in these fields are computed by implementing a collocation error estimation (*Awange et al.*, 2016; *Ferreira et al.*, 2016) using TWSC estimates from the CSR, Jet Propulsion Laboratory (JPL), and GeoForschungsZentrum (GFZ) L2 data. To compute basin averages within a region of interest e.g., various states, the leakage reduction and averaging approach in *Khaki et al.* (2018) is used, which simultaneously minimizes the summation of leakage-in and leakage-out contributions.

2.3. In-situ USGS groundwater and ESA CCI satellite derived soil data

In-situ groundwater level data are provided by the US Geological Survey (USGS) groundwater network [5], which contains a record of groundwater levels between 1970-now for ∼ 100000 wells across the country. For this study, the point-wise data for 2003-2017 are downloaded, but we exclude measurements with large data gaps, and those without seasonal variations. Selected groundwater levels (∼ 58800 wells) are then temporally averaged to produce monthly time series.

[4] http://www2.csr.utexas.edu/grace/
[5] https://water.usgs.gov/ogw/networks.html

The stations located in each $0.125° \times 0.125°$ grid are spatially averaged to produce a time series that is comparable to the W3RA model outputs. Converting in-situ groundwater level data (GWL) to groundwater storage (GWS) changes requires data on the Storage coefficient (Sc), where $GWS = Sc \times GWL$. Determining Sc is quite difficult because it is not a simple geologic parameter and it can hardly be determined by pumping tests, therefore, different approaches have been introduced to approximate it regionally. For example *Rodell et al.* (2007) applied an average value of 0.15 in the Mississippi River basin, and *Xiao et al.* (2015) used a range of 0.02 to 0.6 in the Mid-Atlantic Region of the CONUS based on the technical insights provided by USGS. However, since the Sc estimates are only available for some regions, for the entire CONUS, the USGS groundwater level data are standardized by subtracting their temporal mean and dividing the residuals by their standard deviations. These values are then used to evaluate the W3RA and the MCMC-DA derived standardized groundwater storage estimates (see Section 4.1.3). Comparisons in terms of water storage are performed for Texas and California, where data on storage coefficients are available from previous studies, i.e., High Plain aquifer within Texas, *Gutentag et al.* (2014), and Central Valley aquifer within California, *Scanlon et al.* (2012b). The average Sc in these regions are reported to be 0.18, and 0.15, respectively.

ESA CCI soil moisture product (*Gruber et al.*, 2019) is used in this study to validate the top layer (< 10 cm) soil water storage of W3RA and those from MCMC-DA. The latest release (v04.7) of daily ESA CCI with the spatial resolution of $0.25° \times 0.25°$ covering the period of 2003-2017 is downloaded from the ESA website[6]. Monthly ESA CCI soil moisture time series are computed by the temporal averaging of daily products. These values are then spatially interpolated (using a linear interpolation, *Meijering*, 2002) on the same $0.125° \times 0.125°$ grids as in W3RA and MCMC-DA. The volumetric units (m^3 m^{-3}) of the ESA CCI is converted to the vertical changes in soil water storage (in mm) using a weighted averaging of the first 2 layers (0-5 cm, 5-10 cm) of the STATSGO porosity values [7].

3. Method

A Bayesian Marcov Chain Monte Carlo-Data Assimilation (MCMC-DA) approach is formulated in this study as a multi-variate 'state-space model' (*Bernstein*, 2005), which can be used to recursively update individual water storage components from the W3RA (as a priori information) with GRACE TWSC (as observations). This implementation allows both state parameters and error covariance matrix of the additive innovations to vary in time. Within the procedure of MCMC-DA, the unknown state parameters and temporal dependency between them are estimated using the MCMC (*Geyer*, 1991; *Gilks et al.*, 1996) algorithm. The solution to recursively update the prior value of the unknown parameters is approximated by the Gibbs sampling (*Gelfand and Smith*, 1990; *Smith and Roberts*, 1993), where the joint posterior distribution of the unknown parameters is estimated using the forward-filtering backward-smoothing recursion approach as in *Kitagawa* (1987). In the ESM, we provide the detailed description of MCMC-DA, its implementation, and its differences with the DMDA formulation (*Mehrnegar et al.*, 2020), where the latter is previously used for merging an ensemble of water storage simulations from multi-model outputs and GRACE TWSC.

[6] http://www.esa-soilmoisture-cci.org
[7] http://www.soilinfo.psu.edu/

4. Results and Discussion

In this section, before concentrating on the results of MCMC-DA and their evaluation with independent data, we provide an overview of the comparison of variance between GRACE TWSC (used as observations) and W3RA (whose individual water storage estimates are used as a priori information in the MCMC-DA approach). Long-term linear trend and annual-amplitude of TWSC derived from GRACE and W3RA are shown in Fig. ESM.2 of ESM- Section 2. The results show large differences in the linear trend within the west and south of the CONUS, e.g., California and Texas, that are influenced by irrigation and drought (*Famiglietti et al.*, 2011; *Scanlon et al.*, 2012a; *Rodell et al.*, 2018), and within the northern CONUS, that are influenced by high-intensity rainfall and flooding events (e.g., the 2011's flood in the Missouri River, *Zhang and Schilling*, 2006; *Zheng et al.*, 2014; *Reager et al.*, 2014). Large differences in the annual-amplitude of TWSC are found within the Great Lakes and in the southeastern CONUS. In contrast, the annual-amplitude of W3RA TWSC within Florida is much greater than that estimated by GRACE TWSC (for more details please see ESM- Section 2). The differences in the seasonality of TWSC, between modeled and measured, can be related to errors in the forcing data and uncertainty in model parameters that control these values (*Van Dijk*, 2010; *Van Dijk et al.*, 2011), which is the case for most available models as demonstrated by *Scanlon et al.* (2018) and *Mehrnegar et al.* (2020). Comparison between GRACE and W3RA TWSC indicates that GRACE TWSC has the potential to be used for modifying the W3RA's water storage simulations in terms of long-term trends and seasonality. We will also show that the modification is even beyond these components and some climate modes, such as that of ENSO, are influenced after implementing MCMC-DA.

In what follows, we assess the performance of MCMC-DA in estimating individual water storage changes. The focus is to explore changes in groundwater, which is important for water resources, and by integrating GRACE data into the model, we aim to introduce the model's missing trends in the groundwater compartment. We also evaluate the soil water storage (top layer $< 10cm$), which is important to understand the land-atmosphere interactions (*Levine et al.*, 2016; *Brocca et al.*, 2017). Besides, previous Data Assimilation (DA) attempts (*Girotto et al.*, 2016) showed that a single GRACE DA might introduce unrealistic signals to the soil water storage compartments. Therefore, here, we examine whether such errors can be avoided using MCMC-DA, where the uncertainties and the dynamic evolution of water states are rigorously accounted for. It is worth mentioning here that the DMDA approach (*Mehrnegar et al.*, 2020) is also used to integrate GRACE TWSC into W3RA, and the obtained groundwater and soil water storage are compared with those of MCMC-DA. The DMDA results are also validated against independent ESA CCI and USGS data (results are not shown here). The numerical results indicate that, compared to DMDA, the MCMC-DA estimates are on average 25% closer to the independent estimates. This improvement is likely gained by the dynamic estimation of temporal dependency between unknown state parameters in Eq. (ESM.2) of ESM- Section 1.1 that, compared to DMDA, introduces more realistic updates to the individual water storage components. This is especially true for the top layer soil storage, whose changes are dynamic and strongly coupled to the atmosphere rather than to groundwater changes, where the hydrological memory of the region plays an important role in its evolution. In light of this assessment, we limit our interpretations to those derived from MCMC-DA.

4.1. Groundwater storage changes across the CONUS

Implementing MCMC-DA significantly modifies linear trends, as well as annual and semi-annual amplitudes of groundwater estimates. On average, changes in these components are

found to be in the magnitude of 110%, 25%, 20% of the original W3RA estimates, respectively. In Table 1, we summarize the mean values of linear trends within the CONUS that are estimated based solely on W3RA output versus those using MCMC-DA.

The linear trend and annual-amplitude in groundwater storage are shown in Figs. 1 A1 and A2 and Figs. 1 B1 and B2 for W3RA and MCMC-DA, respectively. Similar plots from the USGS groundwater level observations are shown as an independent comparison in Figs. 1 C1 and C2. We highlight six black boxes in Fig 1 to show the regions with considerable changes after integrating GRACE TWSC into W3RA compared to the original model outputs. The extension of these boxes are reported in Fig 1.

FIGURE 1

TABLE 1

4.1.1. Linear trend of groundwater from MCMC-DA

Pronounced negative trends are found using the MCMC-DA approach in the southwestern (-3.89 ± 0.34 mm/yr, Box 1, California and Nevada) and south-central CONUS (-2.83 ± 0.46 mm/yr, Box 2, Texas, New Mexico, Colorado, Kansas, and Oklahoma). These values are much greater in magnitude than those from the original W3RA results (-1.76 ± 0.54 in Box 1 and -0.10 ± 0.18 mm/yr in Box 2). The USGS groundwater level data (Fig. 1 C1) also show negative trends within these regions (Box 1, -18.39 ± 1.96, and Box 2, -16.55 ± 2.04 mm/yr). Though, the USGS observations are not converted to the storage equivalent, a simple visual comparison between the pattern of trends in Box 1 and 2 of Figs. 1 A1, B1, and C1 indicates that the MCMC-DA trends are more similar to those from the USGS (than the original W3RA). Estimated linear trends of both USGS groundwater level and MCMC-DA groundwater storage are found to be statistically significant within Box 1 and Box 2 based on WMW statistical test results with 99% significance level. These results indicate that the impact of the last decade's droughts that is amplified by intensive irrigation are well reflected in GRACE data (see e.g., *Scanlon et al.*, 2012a; *Mehta et al.*, 2013; *Diffenbaugh et al.*, 2015; *Faunt et al.*, 2016; *Rodell et al.*, 2018) but was not captured by the model as the human water-use component is not included in W3RA. However, this analysis demonstrates that integrating GRACE data to this modeling framework can improve this characterization of variability and trends. In the eastern CONUS (Box 3, including South and North Carolina, Virginia, Georgia, and Tennessee) W3RA shows a systematic negative trend in groundwater storage; however, incorporating GRACE using MCMC-DA adjusts these trends to a mixture of positive and negative values (compare Box 3 in Figs. 1 A1 and B1) with patterns more similar to those from the USGS groundwater level data (see Box 3 in Fig. 1 C1). Analysis for Box 3 indicates that the simple groundwater output of the original W3RA has limitations in accounting for differences in physical parameters of wells in this region, and their different extraction and recharge rates are not well reflected in the model parameters. However, this dynamic complexity is introduced to the groundwater states by implementing the MCMC-DA of GRACE data.

Modification of trends and variability in groundwater storage after implementing MCMC-DA is not limited to the regions with negative trends. In Florida (Box 4), W3RA simulates negative trends (-4.9 ± 0.86 mm/yr) in the north and positive trends ($+2.4 \pm 0.53$ mm/yr) in the south, whereas both MCMC-DA and independent USGS observations indicate trends with opposite signs (MCMC-DA trend in north $+4.3 \pm 0.8$ mm/yr and -1.4 ± 0.4 mm/yr in south). The positive trends in north of the Florida state may be related to considerable inter-annual precipitation in southeastern CONUS (*Dourte et al.*, 2015) and that of south attributed to agricultural expansion and population growth (*Renken et al.*, 2005; *Takatsuka et al.*, 2018).

4.1.2. Impact of the MCMC-DA on seasonality of groundwater storage changes

Seasonal amplitudes (i.e., only annual is shown here) in the MCMC-DA and the original W3RA groundwater storage are similar (differences $< 10\%$ in mm) in almost 75% of the grids across the CONUS. In contrast, large differences are found in Florida (Box 4) and within the Great Lakes area (Box 5), where the high annual-amplitude of W3RA is reduced by $\sim 80\%$ after implementing MCMC-DA (compare Figs. 1 A2 and B2). Similar differences in seasonal amplitudes are apparent between GRACE TWSC and W3RA TWSC (see Fig. ESM.2 in ESM-Section 2). Over-estimation of the seasonal amplitude in the groundwater storage component of W3RA near the Great Lakes (Box 5) may be caused by the model limitations in accounting for surface water changes in the region. Furthermore, in this region, uncertainties of the Glacial Isostatic Adjustment (GIA) model used to reduce the uplift load are big (*Schumacher et al.*, 2018b). This reduction directly affects the estimation of long-term trends in TWSC, and consequently, it alters the individual water storage estimates after MCMC-DA.

The annual and semi-annual amplitudes in MCMC-DA groundwater storage in the southeastern CONUS (Box 6 including Georgia, Alabama, Mississippi, Tennessee, and Kentucky) are estimated to be higher than those from W3RA by more than 55% in mm. These discrepancies are attributed to the high density of vegetation in the southeastern CONUS (see Fig. ESM.3 in ESM- Section 3), where the effect of cool temperatures on the vegetation, and the related vegetation-moisture dynamics cannot be well simulated by W3RA (*Van Dijk*, 2010). Therefore, the seasonal patterns of groundwater storage in evergreen forests of southeastern CONUS are underestimated by the hydrological model.

4.1.3. Numerical validation of groundwater estimates using USGS data

A visual representation of the median, first and third quarterlies of linear trends fitted to unit-less estimates (standardized) of groundwater storage derived from W3RA, MCMC-DA, and USGS data (see Fig. ESM.4 in ESM- Section 3) are shown in Fig. 2 for 20 states across the CONUS. These states are selected within the regions where considerable modifications in estimated groundwater trends are found after implementing MCMC-DA and where we have USGS data from > 38000 wells between 2003 and 2017. The WMW statistical test indicates that the trends of MCMC-DA estimates in Fig. 2 are significantly closer to those of USGS compared to W3RA. Relatively big improvements are detected in California with the median of USGS: 10% MCMC-DA: 8% and W3RA: 3% and relatively smaller changes in Missouri with the median of USGS: 1%, MCMC-DA: 1% and W3RA: 1%.

FIGURE 2

Correlation coefficients between USGS groundwater level and estimated groundwater storage were increased in 76% of the grid points across the CONUS after implementing MCMC-DA. For more details please see Fig. ESM.5 in ESM- Section 4.

4.2. Soil water storage changes across the CONUS

Integrating GRACE data into the model modifies the vertical summation of water storage components (see Eq. (ESM.1 in ESM- Section 1.1). The portion of an update, which is assigned by MCMC-DA to each individual storage compartment, depends on the estimated $\bar{\Theta}$ in Eq. (ESM.10). Our numerical results indicate that the estimated top, shallow, and deep soil layers account for $\sim 14\%$, 28%, and 58% of variance in the total soil water storage, respectively. we find that after implementing MCMC-DA, the magnitude of soil water storage are changed by 72% on average.

Long-term linear trends (22% of the total variance) and annual-amplitude (39% of the total variance) within the top soil layer ($< 10cm$) are shown in Fig. 3, whereas hose of the original W3RA are presented in Figs. 3 A1 and A2, and MCMC-DA in Figs. 3 B1 and B2. Finally, the independent estimates of surface soil storage from the ESA CCI (see Section 2.3) are shown in Figs. 3 C1 and C2, as independent estimates validations.

FIGURE 3

Linear trends in the top soil layer of W3RA (Fig. 3 A1) are found to be small across the CONUS, i.e., less than ± 0.1 mm/yr. Comparing Fig. 3 A1 with B1 indicates that the linear trends are greatly modified after implementing MCMC-DA. Strong negative trends (~ -2 mm/yr) are found in the west (e.g., Box 1, i.e., California and Nevada) and in the south of the country (e.g., Box 2, i.e., Texas, Louisiana, Oklahoma, and New Mexico), while positive trends (up to 2 mm/yr) are found in north of the country (e.g., Box 3, i.e., Montana, Wyoming, North and South Dakota). These estimates are consistent with those from the ESA CCI data, where the linear trends are estimated to be ~ -2, -1.7, and 1.6 mm/yr in Box 1, 2, and 3, respectively.

However, we find differences in estimates within some regions, such as Sierra Nevada and central California (i.e., Box 1), as well as within Louisiana (east of Box 2) where ~ -2 mm/yr declining soil water storage of MCMC-DA is not detected by the ESA CCI product (i.e., -0.14 and 0.95 mm/yr within Sierra Nevada and Louisiana, respectively). The main source of these differences is attributed to the high density of vegetation within the southeastern and northwestern CONUS (see Fig. ESM.3 in ESM- Section 3).

Estimated negative linear trends in the MCMC-DA soil water storage changes within the Louisiana state (Fig. 3 B1, Box 2) are likely associated with the rapid expansion of population and agricultural activities, which have caused replacement of the natural forest lands with crops and modern vegetation landscapes (*Conroy et al.*, 2003; *Sun*, 2013). Removal of tree cover from forest and woodland soils may increase runoff and erosion rates, which in turn may decrease soil infiltration capacity (*Doerr and Thomas*, 2000; *Ferreira et al.*, 2000; *Benito et al.*, 2003). Furthermore, a large area of the western CONUS, in California and western Nevada, has experienced severe forest fires during the last decades, which influenced ecosystem properties, such as forest fragmentation, soil erosion rates, and sedimentation (*Agee*, 1996; *Beaty and Taylor*, 2007; *Miller et al.*, 2009). GRACE satellites are able to detect large-scale changes in water storage components, such as those related to massive changes in vegetation, which are successfully introduced into the MCMC-DA soil water storage estimates within these regions. ESA CCI product is, however, sensitive to the surface roughness and vegetation density parameter, which affects the quality of these data within the forest regions (*Dorigo et al.*, 2017).

W3RA soil water storage shows high seasonality in the west and northwest of the CONUS (Fig. 3 A2, Box 4), where MCMC-DA decreases this value by $\sim 42\%$ on average (Fig. 3 B2, Box 4). These values are found to be similar to those of ESA CCI (see Fig. 3 C2) in 76% of grid points across the CONUS with differences $<\sim 5$ mm. In the southeastern CONUS, where considerable inter-annual precipitation is expected (*Dourte et al.*, 2015), the magnitude of the annual-amplitude in the W3RA soil water storage is estimated to be less than a few millimeters (see Fig. 3 A2, Box 5). This is due to the fact that the effect of cool temperatures on vegetation, and the related vegetation-moisture dynamics cannot be simulated well by W3RA (*Van Dijk*, 2010). Therefore, seasonal patterns in evergreen forests are underestimated. After implementing MCMC-DA, this value increases up to ~ 21 mm (Fig. 3 B2, Box 5), which is closer to the ESA CCI value of ~ 16 mm (Fig 3 C2). Temporal correlation coefficients and the Root Mean Squares of Differences (RMSD) between ESA CCI soil moisture product and

the top-layer soil water changes derived from W3RA and MCMC-DA (Fig ESM.6) indicate average improvements of 67% and 73%, respectively, within CONUS, where positive correlation coefficients (higher than 0.6) are found within 90% of the CONUS between the ESA CCI and both W3RA and MCMC-DA estimates. For more details please see ESM- Section 5.

4.3. Impact of ENSO on groundwater and soil water storage changes across the CONUS

To demonstrate that how GRACE TWSC might alter the inter- and intra-annual components of water storage changes, we extract the dominant ENSO mode from MCMC-DA and W3RA water storage components and compare them with climate indices (see e.g., *Anyah et al.*, 2018) in terms of temporal correlation coefficients with the El Niño Southern Oscillation (ENSO). To this end, the Independent Component Analysis (ICA, *Forootan and Kusche*, 2012, 2013; *Forootan et al.*, 2018) is applied to isolate the ENSO modes from monthly W3RA and MCMC-DA groundwater and soil water storage outputs. The results are then compared in terms of amplitude and correlation coefficients with the ENSO index (Niña 3.4 index [8]). Details about the ICA approach and extracting the ENSO modes of water storage are reported in ESM- Section 6.

ICA is applied to the groundwater storage and soil water storage estimates to MCMC-DA after removing the long-term linear trend and seasonality (shown in Figs. 1 and 3). The first two dominant ICA modes are shown in Figs. 4 and 5, where the spatial anomaly modes are from the MCMC-DA estimates. The associated temporal patterns (that are statistically independent and marked as IC1 and IC2 in Figs. 4 and 5) are estimated by projecting the MCMC-DA and W3RA data onto the anomaly maps. These modes correspond to 15% and 13% of the residual groundwater, as well as 13% and 10% of the residual soil water storage variability, respectively. For comparison the Niña 3.4 index and its Hilbert transform are shown alongside the temporal components. We find that the IC1 derived from both groundwater and soil water storage is in phase with the ENSO index, while IC2 follows its out-of-phase evaluation, i.e., the Hilbert transformation of the ENSO index. Therefore, these two modes capture the dominant influence of ENSO on groundwater and soil water storage changes across the CONUS, covering 2003-2017. The numerical results indicate that correlation coefficients between the ICs and the ENSO index are greatly increased after integrating the GRACE TWSC estimates into W3RA. For example, agreement between IC1 and IC2 of W3RA groundwater storage and the ENSO index (Fig. 4) are increased from 0.34 to 0.56 (65% improvement) and from 0.18 to 0.45 (170% improvement) using MCMC-DA, respectively. Similar behaviour is found in the soil water compartment, where the temporal correlation coefficients are increased from 0.21 to 0.64 for IC1 and from 0.11 to 0.49 for IC2 (Fig. 5).

FIGURE 4

FIGURE 5

An independent comparison is performed by applying ICA on monthly precipitation data from ERA-Interim[9]. As expected, the first two independent modes of the linearly de-trended and de-seasonalized time series of precipitation correspond to the ENSO mode. Correlation coefficients between IC1 and the ENSO index (0.67), and between IC2 and the Hilbert ENSO

[8] https://www.esrl.noaa.gov/psd/data/correlation/nina34.data

[9] https://apps.ecmwf.int/datasets/data/interim-full-daily/levtype=sfc/

index (0.43) are high (Fig. 6). Higher similarities are found between ENSO modes of soil and precipitation (correlation coefficient of 0.58) than those of between groundwater and precipitation (correlation coefficient of 0.41). This indicates that the coupling between shallow storage and precipitation is stronger than that of the storage changes in the groundwater compartment and precipitation.

FIGURE 6

La Niña events resulted in water deficits in the southwest and southeast of the CONUS (including parts of Texas, Louisiana, Arkansas, Mississippi, Alabama, and Georgia) as shown by the comparison of ENSO modes of MCMC-DA groundwater and soil water storage (Fig. 4 and Fig. 5), and those of precipitation anomaly (Fig. 6) (*Cook et al.*, 2007; *Manuel*, 2008; *Seager et al.*, 2014; *Rippey*, 2015). In contrast, wetter than normal conditions are detected in the northwest, e.g., the 2011's Missouri River floods (*Zheng et al.*, 2014; *Reager et al.*, 2014). Both W3RA and MCMC-DA capture the influence of La Niña events on groundwater storage changes across the CONUS, especially those between 2010-2014 (Fig. 4). However, the ENSO mode of W3RA soil water storage shows an opposite evolution compared to that of the ENSO index during these years. This is, however, modified after implementing the MCMC-DA approach, where a correlation coefficient of 0.72 is found between IC1 and the ENSO index (Fig. 5).

4.4. Down-scaling GRACE TWSC observation using MCMC-DA

MCMC-DA is able to down-scale GRACE TWSC observations vertically (separating to individual storage estimates) and horizontally (i.e., improving the $\sim$ 300 km resolution to $\sim$ 12.5 km). To illustrate this gain, a latitudinal (the longitude is fixed at $-100°$) and a longitudinal (latitude is fixed at $40°$) profiles are shown in Fig. 7 left and right panels, respectively. Here, we only show the changes in the linear trends fitted to the GRACE TWSC, as well as to the W3RA and MCMC-DA groundwater and soil water estimates. The GRACE signal evolves quite smoothly (see the solid black lines), but those of W3RA and MCMC-DA represent spatially-dependent variability. Integrating GRACE TWSC into W3RA using MCMC-DA, however, modifies the evolution of both soil and groundwater storage estimates. In the left panel (i.e., longitude profile), the larger portion of the storage update is introduced to the groundwater compartment (compare the light- and dark-blue curves), where the profile is modified towards GRACE. The soil water storage profile is only modified marginally (i.e., standard deviations of the update is 36% of groundwater). We find similar magnitudes of updates to soil water and groundwater storage with the standard deviations of 1.14 mm and 2.46 mm, respectively (see Fig. 7 right panel). The results therefore indicate that the MCMC-DA considers the magnitude of storage in various compartments to modify them and the updated estimates can be used to explore high-resolution hydrological changes across the CONUS as demonstrated in previous sections. More detailed results are also provided in Section 4.5.

FIGURE 7

4.5. Changes in water storage components in regions with considerable differences between MCMC-DA and W3RA model outputs

In what follows, we explore changes in the water storage components within Texas and California where considerable differences are found between the MCMC-DA and W3RA estimates (see Section 4.1 and Section 4.2). Comparisons are provided in terms of the spatial distribution of trends, and spatially averaged groundwater and soil water storage changes within these

states. Because the storage coefficients (Sc) are available for these states from previous studies, an evaluation in terms of groundwater storage is presented. Complementary comparisons are provided with the soil storage using ESA CCI data, as well as precipitation anomalies, and the Palmer Hydrological Drought Index [10] (PHDI, *Palmer*, 1965).

4.5.1. Changes in water storage components within Texas

Texas (located in the southcentral CONUS) is the second largest state in the country by area (after Alaska) and population (after California). According to the Office of the State Demographer and the Texas State Data Center's 2014 predictions, its population is projected to increase until 2050 (*Potter and Hoque*, 2014).

Texas experienced several drought events during the last 2 decades with those of 2010-2014 being the strongest (Fig. 8 A, *Long et al.*, 2013). The ENSO modes of the MCMC-DA groundwater (Fig. 4) and soil water storage (Fig. 5), as well as those of precipitation anomaly (6), indicate that La Niña events are the main climatological cause of these droughts (see also *Seager et al.*, 2014; *Rippey*, 2015). This is well reflected in the magnitude of precipitation anomalies (Fig. 8 B), where the annual precipitation is substantially reduced by 56% during the drought years of 2010-2014. This is also well reflected in the averaged GRACE TWSC and MCMC-DA TWSC in Fig. 8 C, where the evolution closely follows the PHDI (with the correlation coefficient of 0.75) showing that this integration improves representation of drought events.

USGS groundwater storage within Texas is obtained by averaging the observed levels and using an average storage coefficient (i.e., 0.18, see Section 2.3) for the conversion. The results (the dark green curve in Fig. 8 D) indicate that during the extreme drought of 2010-2014, the mean of groundwater storage in Texas markedly decreased (-36 mm) compared to the mean value of 2003-2010. Comparing groundwater storage estimates of the original W3RA and MCMC-DA with those of USGS, indicates a higher agreement after integrating GRACE data (i.e., Root Mean Squares of Differences, RMSD, reduced from 60 mm to 18 mm).

Earlier in Fig. 3 A, it appears that the original W3RA simulates soil water storage with a negligible linear trend within the entire CONUS. Integration of GRACE TWSC into W3RA model outputs introduces a negative linear trend to the soil compartment, and modifies its cyclic components (such as seasonality). This is reflected in the averaged soil storage time series (Fig. 8 E), where the evolution of MCMC-DA is found to be closer to ESA CCI with the correlation coefficient of 0.56 compared to that of the original W3RA (i.e., 0.32). The standard deviation of storage is also modified from 16.56 mm to 26.63 mm after integrating GRACE TWSC.

FIGURE 8

4.5.2. Changes in water storage components within California

California is the third largest (by area) and most densely populated state, which ranks first in the country in terms of economical activities and agricultural value. California has various types of climate from hyper-arid to polar, depending on latitude, elevation, and proximity to the coast. PHDI in Fig. 9 A, precipitation anomalies in Fig. 9 B, and TWSC observed by GRACE mission in Fig. 9 C indicate that California has experienced several drought events during the last decades such as the three-year drought of 2007-2009 (*Jones*, 2010) and the five-year drought between 2012-2017 (see e.g., *Griffin and Anchukaitis*, 2014; *Seager et al.*, 2015;

[10] https://www.ncdc.noaa.gov/temp-and-precip/drought/historical-palmers/

Diffenbaugh et al., 2015).

The averaged GRACE TWSC estimates indicates that during 2012-2017, the state lost TWSC at the rate of -22.50 mm/yr. Large differences are found between the original W3RA and GRACE TWSC during these drought years (RMSD of 54.51 mm) indicating that in addition to the precipitation deficit (−10.45 mm/yr) anthropogenic modifications contributed strongly in the water storage decline (−12.05 mm/yr).

In Fig. 9 D, the averaged groundwater storage changes within California are shown. The USGS water levels are converted to storage estimates using an average Sc of 0.15 from *Scanlon et al.* (2012b). We show the averaged soil water storage results in Fig. 9 E with a comparison with the ESA CCI products. Comparing the curves in Fig. 9 D with Fig. 9 E indicates that on 77% of the update from GRACE TWSC is introduced to the groundwater compartment. A decreasing trend of −4.95 mm/yr is derived for groundwater storage during 2003-2017 and −18.9 mm/y for the drought period of 2012-2017. These estimates are found to be close to that from USGS data, i.e., −3.46 mm/yr during 2003-2017 and −17.79 mm/yr during 2012-2017. GRACE data have mostly modified the linear trend in the soil water storage changes (see Fig. 9 E), i.e., changing from −0.45 mm/yr to −1.66 mm/yr, which is closer to that of ESA CCI (−1.12 mm/yr).

FIGURE 9

5. Summary and Conclusions

In this study, a novel Bayesian Markov Chain Monte Carlo-based Data Assimilation (MCMC-DA), is introduced to integrate GRACE TWSC into individual water storage components of the W3RA water balance model, considering the error structure of the model simulations and the GRACE TWSC as observations. This integration is performed to explore meso-scale (∼12.5 km) groundwater and soil water storage changes across the CONUS, covering 2003-2017. This approach is tested by performing various comparisons between the original W3RA estimates and the MCMC-DA results, as well as validations against the in-situ US Geological Survey (USGS) groundwater level observations and the European Space Agency (ESA)'s Climate Change Initiative (CCI) soil moisture products between 2003-2017. The numerical results indicate that MCMC-DA performs well in introducing long-term linear trends and modifying the seasonality of the W3RA's groundwater (Section 4.1) and soil water storage (Section 4.2) within CONUS. The statistical measures show an improvement, e.g., in terms of both temporal correlation coefficients and the Root Mean Squares of Differences (RMSD) after implementing the MCMC-DA relative to the original W3RA results (see Section ESM- Section 4 and ESM- Section 5). For example, assimilating GRACE TWSC into W3RA amplifies trends in groundwater storage relative to the original W3RA model outputs as shown by results for Texas and California, where changes in groundwater storage are influenced by both climate variability and change (46%), as well as anthropogenic modifications (54%). To demonstrate the impact of integrating GRACE TWSC into W3RA on the inter- and intra-annual components of water storage changes, we also investigate the storage changes associated to the El Niño Southern Oscillation (ENSO). For this, the Independents Component Analysis (ICA) is applied to isolate the ENSO modes from groundwater and soil water storage estimates. The modes derived from MCMC-DA are found to be better correlated to the Niña 3.4. ENSO index. Comparisons of ENSO modes of water storage show that MCMC-DA improve agreement between soil water and precipitation (correlation coefficient of 0.58), relative to W3RA (correlation coefficient of 0.41). This indicates that the coupling procedure between the shallow soil water storage and precipitation is

stronger than that of the deep storage changes associated with the groundwater compartment. Comparing W3RA and MCMC-DA TWSC (e.g., the red and blue curves in Fig. 8 C) indicates that integrating GRACE data into W3RA modifies the timing of water storage changes (i.e., on average it advances the phase of the W3RA TWSC time series by 2 months). Therefore, we conclude that the proposed integration of GRACE data into W3RA improved representation of slowly evolving hydrological processes, such as hydrological droughts (see e.g., *Forootan et al.*, 2019).

In this study, GRACE L2 (Level 2) product are applied to estimate GRACE TWSC to be used as observations in the MCMC-DA procedure (see Section 2.2). It is known to the science community that though there are similarities in overall patterns of TWSC estimates from existing GRACE solutions (e.g., GRACE L2 and mascon products, *Watkins et al.*, 2015), there are differences in terms of the long-term trends and the seasonal magnitudes. These differences are more pronounced in coastal regions such as the southeast CONUS. In general, there is no proof to select the best gravity recovery technique for coastal regions, that is why alternative inversion techniques are being developed (*Ferreira et al.*, 2020). For example in *Yang et al.* (2017), it is shown that the gravity solutions that consider sea level equation might work the better compared to the existing GRACE products. However, an up-to-date product that covers the study period is not available. From the obtained results in this study, we find that MCMC-DA introduces long-term trends to the groundwater storage in the southeast of CONUS (see Fig. 1). However, the magnitude of this update could have been bigger if the mascon solution was used instead. Therefore, the influence of using various GRACE products on the MCMC-DA estimations will be subject to future investigations.

Our results show that estimating groundwater and soil water storage over the Great Lakes area is considerably complex. This may be due to its limitations in accounting for the interactions between surface water and groundwater in regions with the predominant influence of surface water (e.g., the Great Lakes). Furthermore, over the northern part of CONUS the uncertainties of GIA models, to reduce the effect of post-glacial rebound from GRACE TWSC estimates, are big (*Schumacher et al.*, 2018b). Since this reduction directly affects the estimation of long-term trends in TWSC and consequently it alters the individual water storage estimates after MCMC-DA, in future, the MCMC-DA may be extended to constrain both water balance and surface deformation.

Acknowledgments

We would like to thank the Associated Editor Dr. José Virgílio Cruz and two anonymous reviewers whose comments were used to improve the quality of this manuscript. The authors acknowledge the usage of data products: GRACE L2 from CSR, USGS, ESA-CCI, ERA-Interim, W3RA, and PHDI that were provided to this study free of charge. N. Mehrnegar would like to thank the Vice Chancellor's international scholarship for her PhD fund.

References

Agee, J. K. (1996), *Fire ecology of Pacific Northwest forests*, Island press.

Anyah, R. O., E. Forootan, J. L. Awange, and M. Khaki (2018), Understanding linkages between global climate indices and terrestrial water storage changes over Africa using GRACE prod, *Science of The Total Environment*, *635*, 1405–1416, doi:10.1016/j.scitotenv.2018.04.159.

Awange, J. L., E. Forootan, M. Kuhn, J. Kusche, and B. Heck (2014), Water storage changes and climate variability within the Nile Basin between 2002 and 2011, *Advances in Water Resources*, *73*, 1–15, doi:10.1016/j.advwatres.2014.06.010.

Awange, J. L., V. Ferreira, E. Forootan, Khandu, S. Andam-Akorful, N. Agutu, and X. He (2016), Uncertainties in remotely sensed precipitation data over Africa, *International Journal of Climatology*, *36*(1), 303–323, doi:10.1002/joc.4346.

Barnston, A. G., and R. E. Livezey (1987), Classification, seasonality and persistence of low-frequency atmospheric circulation patterns, *Monthly weather review*, *115*(6), 1083–1126, doi:10.1175/1520-0493(1987)115⟨1083:CSAPOL⟩2.0.CO;2.

Beaty, R. M., and A. H. Taylor (2007), Fire disturbance and forest structure in old-growth mixed conifer forests in the northern Sierra Nevada, California, *Journal of Vegetation Science*, *18*(6), 879–890, doi:10.1111/j.1654-1103.2007.tb02604.x.

Benito, E., J. Santiago, E. de Blas, and M. Varela (2003), Deforestation of water- repellent soils in Galicia (NW Spain): effects on surface runoff and erosion under simulated rainfall, *Earth Surface Processes and Landforms*, *28*(2), 145–155, doi:10.1002/esp.431.

Bernstein, D. S. (2005), *Matrix mathematics: theory, facts, and formulas with application to linear systems theory*, vol. 41, Princeton university press Princeton.

Bolten, J. D., W. T. Crow, X. Zhan, T. J. Jackson, and C. A. Reynolds (2009), Evaluating the utility of remotely sensed soil moisture retrievals for operational agricultural drought monitoring, *IEEE Journal of Selected Topics in Applied Earth Observations and Remote Sensing*, *3*(1), 57–66, doi:10.1109/JSTARS.2009.2037163.

Brocca, L., L. Ciabatta, C. Massari, S. Camici, and A. Tarpanelli (2017), Soil moisture for hydrological applications: open questions and new opportunities, *Water*, *9*(2), 140, doi:10.3390/w9020140.

Castellazzi, P., R. Martel, A. Rivera, J. Huang, G. Pavlic, A. I. Calderhead, E. Chaussard, J. Garfias, and J. Salas (2016), Groundwater depletion in Central Mexico: Use of GRACE and InSAR to support water resources management, *Water resources research*, *52*(8), 5985–6003, doi:10.1002/2015WR018211.

Chen, J. L., C. R. Wilson, J. S. Famiglietti, and M. Rodell (2007), Attenuation effect on seasonal basin-scale water storage changes from GRACE time-variable gravity, *Journal of Geodesy*, *81*(4), 237–245, doi:10.1007/s00190-006-0104-2.

Chen, J. L., C. R. Wilson, and B. D. Tapley (2010), The 2009 exceptional Amazon flood and interannual terrestrial water storage change observed by GRACE, *Water Resources Research*, *46*(12), doi:10.1029/2010WR009383.

Conroy, M. J., C. R. Allen, J. T. Peterson, L. Pritchard, and C. T. Moore (2003), Landscape Change in the Southern Piedmont: Challenges, Solutions, and Uncertainty Across Scales, *Conservation Ecology*, *8*(2), 3.

Cook, E. R., R. Seager, M. A. Cane, and D. W. Stahle (2007), North American drought: Reconstructions, causes, and consequences, *Earth-Science Reviews*, *81*(1-2), 93–134, doi:10.1016/j.earscirev.2006.12.002.

Dee, D. P., S. M. Uppala, A. Simmons, P. Berrisford, P. Poli, S. Kobayashi, U. Andrae, M. Balmaseda, G. Balsamo, d. P. Bauer, et al. (2011), The ERA-Interim reanalysis: Configuration and performance of the data assimilation system, *Quarterly Journal of the royal meteorological society*, *137*(656), 553–597, doi:10.1002/qj.828.

Dieter, C. A. (2018), *Water availability and use science program: Estimated use of water in the United States in 2015*, Geological Survey.

Diffenbaugh, N. S., D. L. Swain, and D. Touma (2015), Anthropogenic warming has increased drought risk in California, *Proceedings of the National Academy of Sciences*, *112*(13), 3931–3936, doi:10.1073/pnas.1422385112.

Doerr, S. H., and A. D. Thomas (2000), The role of soil moisture in controlling water repellency : new evidence from forest soils in Portugal, *Journal of Hydrology*, *231*, 134–147, doi:10.1016/S0022-1694(00)00190-6.

Dong, X., B. Xi, A. Kennedy, Z. Feng, J. K. Entin, P. R. Houser, R. A. Schiffer, T. L'Ecuyer, W. S. Olson, K.-l. Hsu, et al. (2011), Investigation of the 2006 drought and 2007 flood extremes at the Southern Great Plains through an integrative analysis of observations, *Journal of Geophysical Research: Atmospheres*, *116*(D3), doi:10.1029/2010JD014776.

Dorigo, W., W. Wagner, C. Albergel, F. Albrecht, G. Balsamo, L. Brocca, D. Chung, M. Ertl, M. Forkel, A. Gruber, E. Haas, P. D. Hamer, M. Hirschi, J. Ikonen, R. de Jeu, R. Kidd, W. A. Lahoz, Y. Y. Liu, D. G. Miralles, T. Mistelbauer, N. Nicolai-Shaw, R. Parinussa, C. Pratola, C. Reimer, R. van der Schalie, S. I. Seneviratne, T. Smolander, and P. Lecomte (2017), ESA CCI Soil Moisture for improved Earth system understanding: State-of-the art and future directions, *Remote Sensing of Environment*, *203*, 185–215, doi:https://doi.org/10.1016/j.rse.2017.07.001.

Dourte, D. R., C. W. Fraisse, and W.-L. Bartels (2015), Exploring changes in rainfall intensity and seasonal variability in the Southeastern US: Stakeholder engagement, observations, and adaptation, *Climate Risk Management*, *7*, 11–19, doi:10.1016/j.crm.2015.02.001.

Ducharne, A., R. D. Koster, M. Suarez, M. Stieglitz, and P. Kumar (2000), A catchment-based approach to modeling land surface processes in a general circulation model. II- Parameter estimation and model demonstration, *Journal of Geophysical Research*, *105*, 24, doi:10.1029/2000JD900328.

Eicker, A., E. Forootan, A. Springer, L. Longuevergne, and J. Kusche (2016), Does GRACE see the terrestrial water cycle "intensifying"?, *Journal of Geophysical Research: Atmospheres*, *121*(2), 733–745, doi:10.1002/2015JD023808.

Famiglietti, J. S., M. Lo, S. L. Ho, J. Bethune, K. Anderson, T. H. Syed, S. C. Swenson, C. R. de Linage, and M. Rodell (2011), Satellites measure recent rates of groundwater depletion in California's Central Valley, *Geophysical Research Letters*, *38*(3), doi:10.1029/2010GL046442.

Fasullo, J. T., C. Boening, F. W. Landerer, and R. S. Nerem (2013), Australia's unique influence on global sea level in 2010–2011, *Geophysical Research Letters*, *40*(16), 4368–4373, doi:10.1002/grl.50834.

Fasullo, J. T., D. M. Lawrence, and S. C. Swenson (2016), Are GRACE-era terrestrial water trends driven by anthropogenic climate change?, *Advances in Meteorology*, *2016*, doi:10.1155/2016/4830603.

Faunt, C. C., M. Sneed, J. Traum, and J. T. Brandt (2016), Water availability and land subsidence in the Central Valley, California, USA, *Hydrogeology Journal*, *24*(3), 675–684, doi:10.1007/s10040-015-1339-x.

Ferreira, A. J. D., C. Coelho, R. P. D. Walsh, R. Shakesby, A. Ceballos, and S. Doerr (2000), Hydrological implications of soil water-repellency in Eucalyptus globulus forests, north-central Portugal, *Journal of Hydrology*, *231*, 165–177, doi:10.1016/S0022-1694(00)00192-X.

Ferreira, V. G., H. D. C. Montecino, C. I. Yakubu, and B. Heck (2016), Uncertainties of the Gravity Recovery and Climate Experiment time-variable gravity-field solutions based on three-cornered hat method, *Journal of Applied Remote Sensing*, *10*(1), 1 – 20, doi:10.1117/1.JRS.10.015015.

Ferreira, V. G., B. Yong, K. Seitz, B. Heck, and T. Grombein (2020), Introducing an Improved GRACE Global Point-Mass Solution—A Case Study in Antarctica, *Remote Sensing*, *12*(19), 3197, doi:10.3390/rs12193197.

Flechtner, F., K.-H. Neumayer, C. Dahle, H. Dobslaw, E. Fagiolini, J.-C. Raimondo, and A. Güntner (2016), What can be expected from the GRACE-FO laser ranging interferometer for Earth science applications?, *Surveys in Geophysics*, *33*(2), 453–470, doi:10.1007/s10712-015-9338-y.

Forootan, E., and J. Kusche (2012), Separation of global time-variable gravity signals into maximally independent components, *Journal of Geodesy*, *86*(7), 477–497, doi:0.1007/s00190-011-0532-5.

Forootan, E., and J. Kusche (2013), Separation of deterministic signals using independent component analysis (ICA), *Studia Geophysica et Geodaetica*, *57*(1), 17–26, doi:10.1007/s11200-012-0718-1.

Forootan, E., O. Didova, M. Schumacher, J. Kusche, and B. Elsaka (2014a), Comparisons of atmospheric mass variations derived from ECMWF reanalysis and operational fields, over 2003–2011, *Journal of Geodesy*, *88*(5), 503–514, doi:10.1007/s00190-014-0696-x.

Forootan, E., R. Rietbroek, J. Kusche, M. A. Sharifi, J. L. Awange, M. Schmidt, P. Omondi, and J. Famiglietti (2014b), Separation of large scale water storage patterns over Iran using GRACE, altimetry and hydrological data, *Remote Sensing of Environment*, *140*, 580–595, doi:10.1016/j.rse.2013.09.025.

Forootan, E., R. Rietbroek, J. Kusche, M. A. Sharifi, J. L. Awange, M. Schmidt, P. Omondi, and J. S. Famiglietti (2014c), Separation of large scale water storage patterns over Iran using GRACE, altimetry and hydrological data, *Remote Sensing of Environment*, *140*, 580–595, doi:10.1016/j.rse.2013.09.025.

Forootan, E., J. L. Awange, M. Schumacher, R. O. Anyah, A. I. J. M. van Dijk, J. Kusche, et al. (2016), Quantifying the impacts of ENSO and IOD on rain gauge and remotely sensed precipitation products over Australia, *Remote sensing of Environment*, *172*, 50–66, doi:10.1016/j.rse.2015.10.027.

Forootan, E., A. Safari, A. Mostafaie, M. Schumacher, M. Delavar, and J. L. Awange (2017), Large-scale total water storage and water flux changes over the arid and semiarid parts of the Middle East from GRACE and reanalysis products, *Surveys in Geophysics*, *38*(3), 591–615, doi:10.1007/s10712-016-9403-1.

Forootan, E., J. Kusche, M. Talpe, C. K. Shum, and M. Schmidt (2018), Developing a Complex Independent Component Analysis (CICA) Technique to Extract Non-stationary Patterns from Geophysical Time Series, *Surveys in Geophysics*, *39*(3), 435–465, doi:10.1007/s10712-017-9451-1.

Forootan, E., M. Khaki, M. Schumacher, V. Wulfmeyer, N. Mehrnegar, A. Van Dijk, L. Brocca, S. Farzaneh, F. Akinluyi, G. Ramillien, et al. (2019), Understanding the global hydrological droughts of 2003–2016 and their relationships with teleconnections, *Science of the Total Environment*, *650*, 2587–2604, doi:10.1016/j.scitotenv.2018.09.231.

Gelfand, A. E., and A. F. M. Smith (1990), Sampling-based approaches to calculating marginal densities, *Journal of the American statistical association*, *85*(410), 398–409, doi:10.1080/01621459.1990.10476213.

Geyer, C. J. (1991), Markov chain Monte Carlo maximum likelihood.

Gilks, W. R., S. Richardson, and D. J. Spiegelhalter (1996), Introducing markov chain monte carlo, *Markov chain Monte Carlo in practice*, *1*, 19.

Girotto, M., G. J. De Lannoy, R. H. Reichle, and M. Rodell (2016), Assimilation of gridded terrestrial water storage observations from GRACE into a land surface model, *Water Resources Research*, *52*(5), 4164–4183, doi:10.1002/2015WR018417.

Girotto, M., G. J. De Lannoy, R. H. Reichle, M. Rodell, C. Draper, S. N. Bhanja, and A. Mukherjee (2017), Benefits and pitfalls of GRACE data assimilation: A case study of terrestrial water storage depletion in India, *Geophysical research letters*, *44*(9), 4107–4115, doi:10.1002/2017GL072994.

Griffin, D., and K. J. Anchukaitis (2014), How unusual is the 2012–2014 California drought?, *Geophysical Research Letters*, *41*(24), 9017–9023, doi:10.1002/2014GL062433.

Gruber, A., T. Scanlon, R. van der Schalie, W. Wagner, and W. Dorigo (2019), Evolution of the ESA CCI Soil Moisture climate data records and their underlying merging methodology, *Earth System Science Data*, pp. 1–37, doi:10.5194/essd-11-717-2019.

Gutentag, E. D., F. J. Heimes, and N. C. Krothe (2014), *Geohydrology of the High Plains aquifer in parts of Colorado, Kansas, Nebraska, New Mexico, Oklahoma, South Dakota, Texas, and Wyoming*, vol. 1400-B, 63p, doi:10.3133/pp1400B.

Hillel, D. (1998), *Environmental soil physics: Fundamentals, applications, and environmental considerations*, Elsevier.

Houborg, R., M. Rodell, B. Li, R. Reichle, and B. F. Zaitchik (2012), Drought indicators based on model-assimilated Gravity Recovery and Climate Experiment (GRACE) terrestrial water storage observations, *Water Resources Research*, *48*(7), doi:10.1029/2011WR011291.

Illston, B. G., J. B. Basara, and K. C. Crawford (2004), Seasonal to interannual variations of soil moisture measured in Oklahoma, *International Journal of Climatology: A Journal of the Royal Meteorological Society*, *24*(15), 1883–1896, doi:10.1002/joc.1077.

Jones, J. (2010), *California's Drought of 2007-2009: An Overview*, State of California, Natural Resources Agency, California Department of Water resources.

Kalman, R. E. (1960), A new approach to linear filtering and prediction problems, *82*(1), 35–45, doi:10.1115/1.3662552.

Khaki, M., I. Hoteit, M. Kuhn, J. Awange, E. Forootan, A. I. Van Dijk, M. Schumacher, and C. Pattiaratchi (2017), Assessing sequential data assimilation techniques for integrating GRACE data into a hydrological model, *Advances in Water Resources*, *107*, 301–316, doi:10.1016/j.advwatres.2017.07.001.

Khaki, M., E. Forootan, M. Kuhn, J. L. Awange, L. Longuevergne, and Y. Wada (2018), Efficient basin scale filtering of GRACE satellite products, *Remote Sensing of Environment*, *204*, 76–93, doi:10.1016/j.rse.2017.10.040.

Kitagawa, G. (1987), Non-gaussian state—space modeling of nonstationary time series, *Journal of the American statistical association*, *82*(400), 1032–1041, doi:10.1080/01621459.1987.10478534.

Kusche, J., R. Schmidt, S. Petrovic, and R. Rietbroek (2009), Decorrelated GRACE time-variable gravity solutions by GFZ, and their validation using a hydrological model, *Journal of geodesy*, *83*(10), 903–913, doi:10.1007/s00190-009-0308-3.

Kusche, J., A. Eicker, E. Forootan, A. Springer, and L. Longuevergne (2016), Mapping probabilities of extreme continental water storage changes from space gravimetry, *Geophysical Research Letters*, *43*(15), 8026–8034, doi:10.1002/2016GL069538.

Landerer, F. W., and S. C. Swenson (2012), Accuracy of scaled GRACE terrestrial water storage estimates, *Water resources research*, *48*(4), doi:10.1029/2011WR011453.

Leng, G., M. Huang, N. Voisin, X. Zhang, G. R. Asrar, and L. R. Leung (2016), Emergence of new hydrologic regimes of surface water resources in the conterminous United States under future warming, *Environmental Research Letters*, *11*(11), 114,003, doi:10.1088/1748-9326/11/11/114003.

Levine, P. A., J. T. Randerson, S. C. Swenson, and D. M. Lawrence (2016), Evaluating the strength of the land − atmosphere moisture feedback in Earth system models using satellite observations, *Hydrology and Earth System Sciences (Online)*, *20*(12), doi:10.5194/hess-20-4837-2016.

Li, B., M. Rodell, S. Kumar, H. K. Beaudoing, A. Getirana, B. F. Zaitchik, L. G. de Goncalves, C. Cossetin, S. Bhanja, A. Mukherjee, et al. (2019), Global GRACE data assimilation for groundwater and drought monitoring: advances and challenges, *Water Resources Research*, *55*(9), 7564–7586, doi:10.1029/2018WR024618.

Long, D., B. R. Scanlon, L. Longuevergne, A. Y. Sun, D. N. Fernando, and H. Save (2013), GRACE satellite monitoring of large depletion in water storage in response to the 2011 drought in Texas, *Geophysical Research Letters*, *40*(13), 3395–3401, doi:10.1002/grl.50655.

Manuel, J. (2008), Drought in the southeast: lessons for water management, doi:10.1289/ehp.116-a168.

Maupin, M. A., J. F. Kenny, S. S. Hutson, J. K. Lovelace, N. L. Barber, K. S. Linsey, et al. (2017), Estimated use of water in the United States in 2010.

Means III, E. G., N. West, and R. Patrick (2005), Population growth and climate change: Will pose tough challenges for water utilities, *Journal-American Water Works Association*, *97*(8), 40–46, doi:10.1002/j.1551-8833.2005.tb07447.x.

Mehrnegar, N., O. Jones, M. B. Singer, M. Schumacher, P. Bates, and E. Forootan (2020), Comparing global hydrological models and combining them with GRACE by dynamic model data averaging (DMDA), *Advances in Water Resources*, *138*, 103,528, doi:10.1016/j.advwatres.2020.103528.

Mehta, V. K., V. R. Haden, B. A. Joyce, D. R. Purkey, and L. E. Jackson (2013), Irrigation demand and supply, given projections of climate and land-use change, in Yolo County, California, *Agricultural water management*, *117*, 70–82, doi:10.1016/j.agwat.2012.10.021.

Meijering, E. (2002), A chronology of interpolation: from ancient astronomy to modern signal and image processing, *Proceedings of the IEEE*, *90*(3), 319–342, doi:10.1109/5.993400.

Miller, J. D., H. D. Safford, M. Crimmins, and A. E. Thode (2009), Quantitative evidence for increasing forest fire severity in the Sierra Nevada and southern Cascade Mountains, California and Nevada, USA, *Ecosystems*, *12*(1), 16–32, doi:10.1007/s10021-008-9201-9.

Miro, M. E., and J. S. Famiglietti (2018), Downscaling GRACE Remote Sensing Datasets to High-Resolution Groundwater Storage Change Maps of California's Central Valley, *Remote Sensing*, *10(1)*, 143, doi:10.3390/rs10010143.

Mo, K. C., L. N. Long, Y. Xia, S. Yang, J. E. Schemm, and M. Ek (2011), Drought indices based on the Climate Forecast System Reanalysis and ensemble NLDAS, *Journal of Hydrometeorology*, *12*(2), 181–205, doi:10.1175/2010JHM1310.1.

Ni, S., J. Chen, C. R. Wilson, J. Li, X. Hu, and R. Fu (2018), Global Terrestrial Water Storage Changes and Connections to ENSO Events, *Surveys in Geophysics*, *39*(1), 1–22, doi:10.1007/s10712-017-9421-7.

Palmer, W. C. (1965), *Meteorological drought*, vol. 30, US Department of Commerce, Weather Bureau.

Peterson, T. C., R. R. Heim Jr, R. Hirsch, D. P. Kaiser, H. Brooks, N. S. Diffenbaugh, R. M. Dole, J. P. Giovannettone, K. Guirguis, T. R. Karl, et al. (2013), Monitoring and understanding changes in heat waves, cold waves, floods, and droughts in the United States: state of knowledge, *Bulletin of the American Meteorological Society*, *94*(6), 821–834, doi:10.1175/BAMS-D-12-00066.1.

Phillips, T., R. S. Nerem, B. Fox-Kemper, J. S. Famiglietti, and B. Rajagopalan (2012), The influence of ENSO on global terrestrial water storage using GRACE, *Geophysical Research Letters*, *39*(16), doi:10.1029/2012GL052495.

Potter, L. B., and N. Hoque (2014), Texas population projections, 2010 to 2050, *Office of the State Demographer*, *4*.

Reager, J. T., B. F. Thomas, and J. S. Famiglietti (2014), River basin flood potential inferred using GRACE gravity observations at several months lead time, *Nature Geoscience*, *7*(8), 588, doi:10.1038/ngeo2203.

Renken, R. A., J. Dixon, J. Koehmstedt, S. Ishman, A. Lietz, R. L. Marella, P. Telis, J. Rogers, and S. Memberg (2005), Impact of anthropogenic development on coastal ground-water hydrology in southeastern Florida, 1900–2000, *US Geol Surv Circ*, *1275*, 77.

Renzullo, L. J., A. Van Dijk, J.-M. Perraud, D. Collins, B. Henderson, H. Jin, A. Smith, and D. L. McJannet (2014), Continental satellite soil moisture data assimilation improves root-zone moisture analysis for water resources assessment, *Journal of Hydrology*, *519*, 2747–2762, doi:10.1016/j.jhydrol.2014.08.008.

Rippey, B. R. (2015), The US drought of 2012, *Weather and Climate Extremes*, *10*, 57–64, doi:10.1016/j.wace.2015.10.004.

Rodell, M., J. Chen, H. Kato, J. S. Famiglietti, J. Nigro, and C. R. Wilson (2007), Estimating groundwater storage changes in the Mississippi River basin (USA) using GRACE, *Hydrogeology Journal*, *15*(1), 159–166, doi:10.1007/s10040-006-0103-7.

Rodell, M., J. S. Famiglietti, D. N. Wiese, J. T. Reager, H. K. Beaudoing, F. W. Landerer, and M.-H. Lo (2018), Emerging trends in global freshwater availability, *Nature*, *557*(7707), 651–659, doi:10.1038/s41586-018-0123-1.

Scanlon, B., Z. Zhang, A. Rateb, A. Sun, D. Wiese, H. Save, H. Beaudoing, M. Lo, H. Müller-Schmied, P. Döll, et al. (2019), Tracking seasonal fluctuations in land water storage using global models and grace satellites, *Geophysical Research Letters*, *46*(10), 5254–5264, doi:10.1029/2018GL081836.

Scanlon, B. R., R. C. Reedy, J. B. Gates, and P. H. Gowda (2010), Impact of agroecosystems on groundwater resources in the Central High Plains, USA, *Agriculture, ecosystems & environment*, *139*(4), 700–713, doi:10.1016/j.agee.2010.10.017.

Scanlon, B. R., C. C. Faunt, L. Longuevergne, R. C. Reedy, W. M. Alley, V. L. McGuire, and P. B. McMahon (2012a), Groundwater depletion and sustainability of irrigation in the US High Plains and Central Valley, *Proceedings of the national academy of sciences*, *109*(24), 9320–9325, doi:10.1073/pnas.1200311109.

Scanlon, B. R., L. Longuevergne, and D. Long (2012b), Ground referencing GRACE satellite estimates of groundwater storage changes in the California Central Valley, USA, *Water Resources Research*, *48*(4), doi:10.1029/2011WR011312.

Scanlon, B. R., Z. Zhang, H. Save, A. Y. Sun, H. M. Schmied, L. P. van Beek, D. N. Wiese, Y. Wada, D. Long, R. C. Reedy, et al. (2018), Global models underestimate large decadal declining and rising water storage trends relative to GRACE satellite data, *Proceedings of the National Academy of Sciences*, *115*(6), E1080–E1089, doi:10.1073/pnas.1704665115.

Schubert, S. D., M. J. Suarez, P. J. Pegion, R. D. Koster, and J. T. Bacmeister (2004), Causes of long-term drought in the US Great Plains, *Journal of Climate*, *17*(3), 485–503, doi:10.1175/1520-0442(2004)017⟨0485:COLDIT⟩2.0.CO;2.

Schumacher, M., J. Kusche, and P. Döll (2016), A systematic impact assessment of GRACE error correlation on data assimilation in hydrological models, *Journal of Geodesy*, *90*(6), 537–559, doi:10.1007/s00190-016-0892-y.

Schumacher, M., E. Forootan, A. I. J. M. van Dijk, H. M. Schmied, R. S. Crosbie, J. Kusche, and P. Döll (2018), Improving drought simulations within the Murray-Darling Basin by combined calibration/assimilation of GRACE data into the WaterGAP Global Hydrology Model, *Remote Sensing of Environment*, *204*, 212–228, doi:10.1016/j.rse.2017.10.029.

Schumacher, M., M. King, J. Rougier, Z. Sha, S. Khan, and J. Bamber (2018b), A new global gps data set for testing and improving modelled gia uplift rates, *Geophysical Journal International*, *214 (3)*, 2164—2176, doi:10.1093/gji/ggy235.

Seager, R., L. M. Goddard, J. A. Nakamura, N. L. Henderson, and D. E. Lee (2014), Dynamical Causes of the 2010/11 Texas_Northern Mexico Drought, *Journal of Hydrometeorology*, *15*(1), 39–68, doi:10.1175/JHM-D-13-024.1.

Seager, R., M. Hoerling, S. Schubert, H. Wang, B. Lyon, A. Kumar, J. Nakamura, and N. Henderson (2015), Causes of the 2011–14 California drought, *Journal of Climate*, *28*(18), 6997–7024, doi:10.1175/JCLI-D-14-00860.1.

Singer, M. B., C. I. Sargeant, H. Piégay, J. Riquier, R. J. Wilson, and C. M. Evans (2014), Floodplain ecohydrology: Climatic, anthropogenic, and local physical controls on partitioning of water sources to riparian trees, *Water resources research*, *50*(5), 4490–4513, doi:10.1002/2014WR015581.

Sinha, D., T. H. Syed, J. S. Famiglietti, J. T. Reager, and R. C. Thomas (2017), Characterizing drought in India using GRACE observations of terrestrial water storage deficit, *Journal of Hydrometeorology*, *18*(2), 381–396, doi:10.1175/JHM-D-16-0047.1.

Slater, L. J., M. B. Singer, and J. W. Kirchner (2015), Hydrologic versus geomorphic drivers of trends in flood hazard, *Geophysical Research Letters*, *42*(2), 370–376, doi:10.1002/2014GL062482.

Smith, A. F. M., and G. O. Roberts (1993), Bayesian computation via the Gibbs sampler and related Markov chain Monte Carlo methods, *Journal of the Royal Statistical Society: Series B (Methodological)*, *55*(1), 3–23, doi:10.1111/j.2517-6161.1993.tb01466.x.

Sun, G. (2013), Impacts of Climate Change and Variability on Water Resources in the Southeast USA, *NCA Southeast Technical Report 204-234*, pp. 210–236, doi:10.5822/978-1-61091-509-0_10.

Swenson, S., D. Chambers, and J. Wahr (2008), Estimating geocenter variations from a combination of GRACE and ocean model output, *Journal of Geophysical Research: Solid Earth*, *113*(B8), doi:10.1029/2007JB005338.

Takatsuka, Y., M. R. Niekus, J. Harrington, S. Feng, D. Watkins, A. Mirchi, H. Nguyen, and M. C. Sukop (2018), Value of irrigation water usage in South Florida agriculture, *Science of The Total Environment*, *626*, 486–496, doi:10.1016/j.scitotenv.2017.12.240.

Tapley, B. D., S. Bettadpur, J. C. Ries, P. F. Thompson, and M. M. Watkins (2004a), GRACE measurements of mass variability in the Earth system, *Science*, *305*(5683), 503–505, doi: 10.1126/science.1099192.

Tapley, B. D., S. Bettadpur, J. C. Ries, P. F. Thompson, and M. M. Watkins (2004b), GRACE measurements of mass variability in the Earth system, *Science*, *305*(5683), 503–505, doi: 10.1126/science.1099192.

Thomas, A. C., J. T. Reager, J. S. Famiglietti, and M. Rodell (2014), A GRACE-based water storage deficit approach for hydrological drought characterization, *Geophysical Research Letters*, *41*(5), 1537–1545, doi:10.1002/2014GL059323.

Trenberth, K. E., and D. P. Stepaniak (2001), Indices of el niño evolution, *Journal of climate*, *14*(8), 1697–1701, doi:10.1175/1520-0442(2001)014⟨1697:LIOENO⟩2.0.CO;2.

Van Dijk, A. (2010), The Australian Water Resources Assessment System: Technical Report 3, Landscape model (version 0.5) Technical Description, CSIRO: Water for a Healthy Country National Research Flagship.

Van Dijk, A., L. J. Renzullo, and M. Rodell (2011), Use of Gravity Recovery and Climate Experiment terrestrial water storage retrievals to evaluate model estimates by the Australian water resources assessment system, *Water Resources Research*, *47*(11), doi:10.1029/2011WR010714.

Van Dijk, A. I. J. M., L. J. Renzullo, Y. Wada, and P. Tregoning (2014), A global water cycle reanalysis (2003–2012) merging satellite gravimetry and altimetry observations with a hydrological multi-model ensemble, *Hydrology and Earth System Sciences*, *18*(8), 2955–2973, doi:10.5194/hess-18-2955-2014.

Wahr, J., and S. Zhong (2012), Computations of the viscoelastic response of a 3-D compressible Earth to surface loading: an application to Glacial Isostatic Adjustment in Antarctica and Canada, *Geophysical Journal International*, *192*(2), 557–572, doi:10.1093/gji/ggs030.

Wahr, J., M. Molenaar, and F. Bryan (1998), Time variability of the earth's gravity field: hydrological and oceanic effects and their possible detection using grace, *Journal of Geophysical Research: Solid Earth*, *108 (B12)*, 30,205–30,229, doi:10.1029/98JB02844.

Watkins, M. M., D. N. Wiese, D.-N. Yuan, C. Boening, and F. W. Landerer (2015), Improved methods for observing Earth's time variable mass distribution with GRACE using spherical cap mascons, *Journal of Geophysical Research: Solid Earth*, *120*(4), 2648–2671, doi:10.1002/2014JB011547.

Xiao, R., X. He, Y. Zhang, V. G. Ferreira, and L. Chang (2015), Monitoring groundwater variations from satellite gravimetry and hydrological models: A comparison with in-situ measurements in the mid-atlantic region of the United States, *Remote Sensing*, *7*(1), 686–703, doi:10.3390/rs70100686.

Yang, F., J. Kusche, E. Forootan, and R. Rietbroek (2017), Passive-ocean radial basis function approach to improve temporal gravity recovery from grace observations, *Journal of Geophysical Research: Solid Earth*, *122*(8), 6875–6892, doi:10.1002/2016JB013633.

Zaitchik, B. F., M. Rodell, and R. H. Reichle (2008), Assimilation of GRACE terrestrial water storage data into a land surface model: Results for the Mississippi River basin, *Journal of Hydrometeorology*, *9*(3), 535–548, doi:10.1175/2007JHM951.1.

Zhang, Y.-K., and K. Schilling (2006), Increasing streamflow and baseflow in Mississippi River since the 1940 s: Effect of land use change, *Journal of Hydrology*, *324*(1-4), 412–422, doi: 10.1016/j.jhydrol.2005.09.033.

Zhang, Z., B. F. Chao, J. Chen, and C. R. Wilson (2015), Terrestrial water storage anomalies of Yangtze River Basin droughts observed by GRACE and connections with ENSO, *Global and Planetary Change*, *126*, 35–45, doi:10.1016/j.gloplacha.2015.01.002.

Zhao, M., I. Velicogna, and J. S. Kimball (2017a), Satellite observations of regional drought severity in the continental United States using GRACE-based terrestrial water storage changes, *Journal of Climate*, *30*(16), 6297–6308, doi:10.1175/JCLI-D-16-0458.1.

Zhao, M., I. Velicogna, and J. S. Kimball (2017b), A global gridded dataset of grace drought severity index for 2002–14: Comparison with pdsi and spei and a case study of the australia millennium drought, *Journal of Hydrometeorology*, *18*(8), 2117–2129, doi:10.1175/JHM-D-16-0182.1.

Zheng, H., D. Barta, and X. Zhang (2014), Lesson learned from adaptation response to Devils Lake flooding in North Dakota, USA, *Regional environmental change*, *14*(1), 185–194, doi: 10.1007/s10113-013-0474-y.

Figures

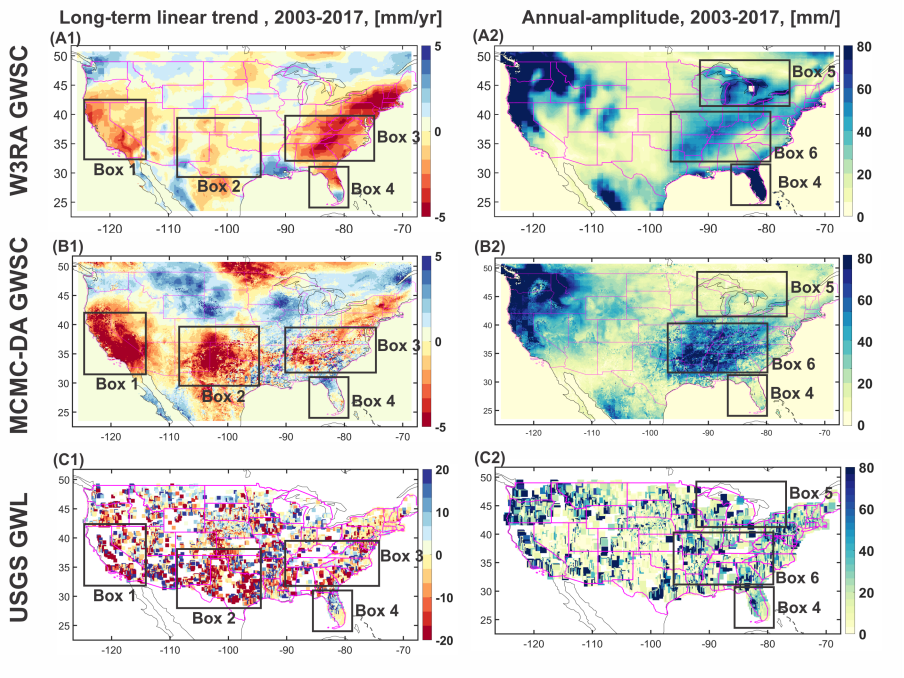

Figure 1: Linear trend and annual-amplitude fitted to the (A1 and A2) groundwater storage changes for the original W3RA; (B1 and B2) groundwater storage estimates from MCMC-DA; and (C1 and C2) the USGS groundwater level observations, expressed in mm/yr, covering the period of 2003-2017. In this figure, the terms GWSC and GWL are used to show groundwater storage changes and groundwater level, respectively. To enhance the visualisation, the black boxes in Fig. 1 (marked as Box 1, 2, 3, 4, 5, and 6) are used to show the regions with considerable groundwater changes after integrating GRACE TWSC into W3RA. The extension of these boxes is reported here as Box 1: [$112^\circ E$_$125^\circ E$, $32^\circ N$_$42^\circ N$], Box 2: [$95^\circ E$_$109^\circ E$, $30^\circ N$_$39^\circ N$], Box 3: [$75^\circ E$_$90^\circ E$, $32^\circ N$_$39^\circ N$], Box 4: [$79^\circ E$_$86^\circ E$, $24^\circ N$_$31^\circ N$], Box 5: [$75^\circ E$_$90^\circ E$, $40^\circ N$_$50^\circ N$], and Box 6: [$79^\circ E$_$97^\circ E$, $30^\circ N$_$40^\circ N$].

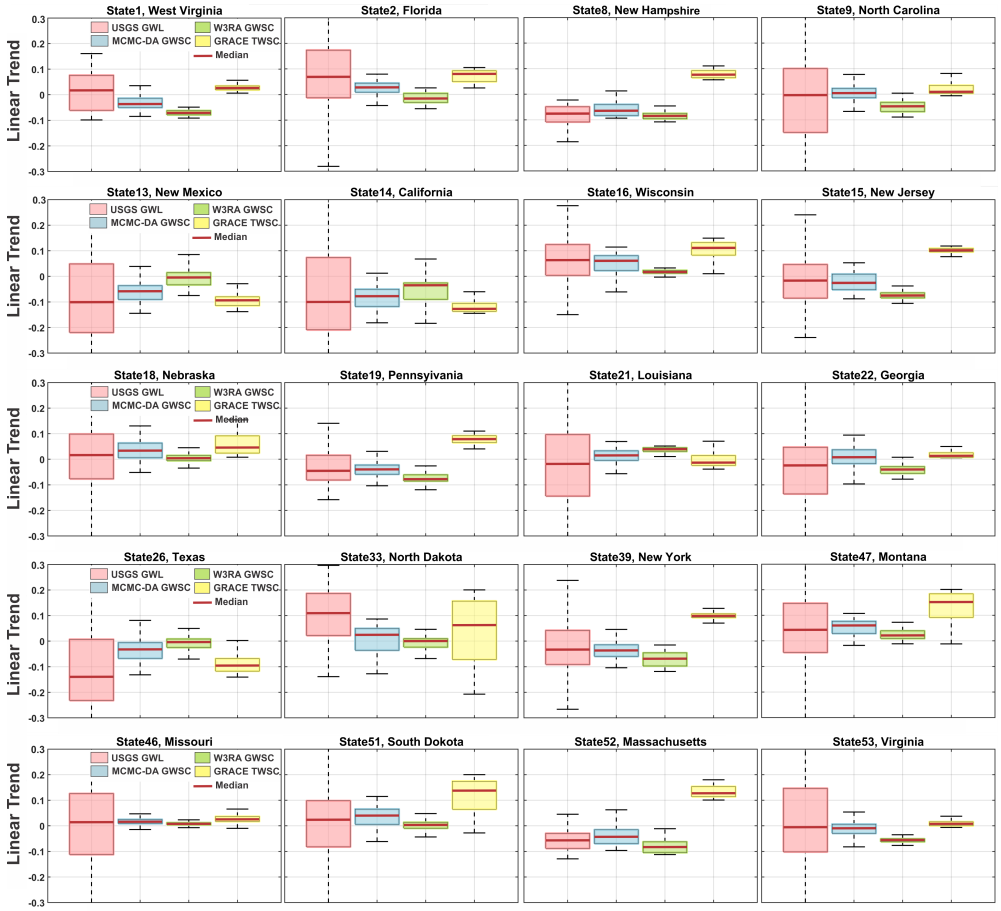

Figure 2: A comparison between the linear trends fitted to the standardize (unit-less) groundwater storage time series from the original W3RA, MCMC-DA groundwater storage, USGS groundwater level observations, and standardize GRACE TWSC within different states of the CONUS, covering the period of 2003-2017. The tops and bottoms of each box are the 25th and 75th percentiles of each data sets (the first and third quartiles), and the red lines show the median of time series. In this figure, the terms GWSC and GWL indicate groundwater storage changes and groundwater level, respectively.

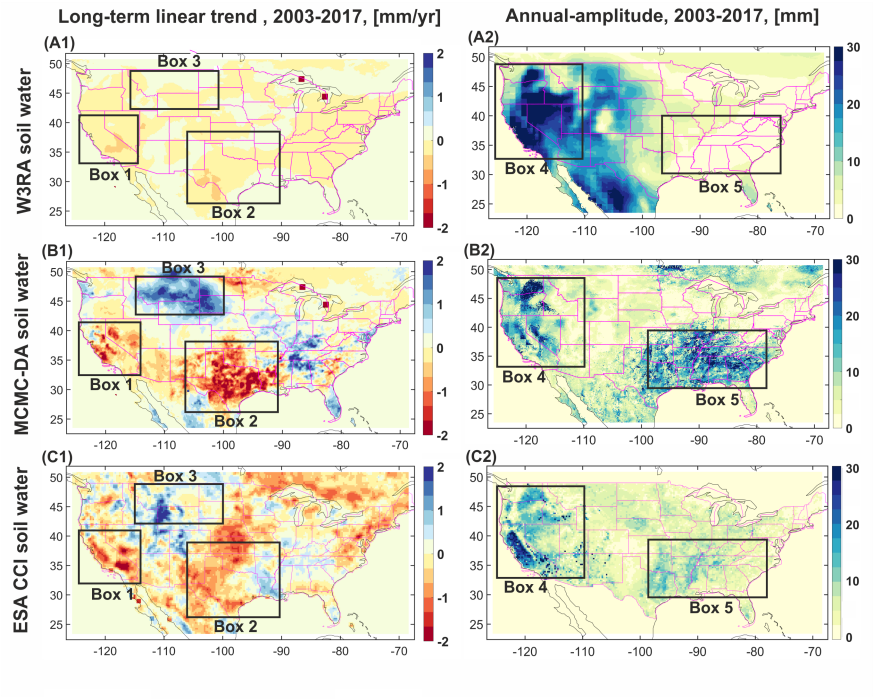

Figure 3: Linear trend and annual-amplitude fitted to (A1 and A2) soil water storage (top-layer, i.e., 10 cm) of the original W3RA; (B1 and B2) the updated soil water storage estimates derived from MCMC-DA; and (C1 and C2) soil water storage estimates from ESA CCI across the CONUS, expressed in mm/yr, and covering 2003-2017. To enhance the visualisation, five boxes are shown in this figure (marked as Box 1, 2, 3, 4, and 5), where considerable changes are detected in the soil compartment after integrating GRACE TWSC into W3RA. The extension of these boxes are reported here as Box 1: [$112^\circ E$_$125^\circ E$, $32^\circ N$_$42^\circ N$], Box 2: [$90^\circ E$_$116^\circ E$, $26^\circ N$_$39^\circ N$], Box 3: [$100^\circ E$_$115^\circ E$, $42^\circ N$_$50^\circ N$], Box 4: [$110^\circ E$_$124^\circ E$, $32^\circ N$_$48^\circ N$], and Box 5: [$75^\circ E$_$90^\circ E$, $30^\circ N$_$40^\circ N$]

Table 1: The mean value of linear trends fitted to the W3RA and MCMC-DA groundwater storage estimates. The results (expressed in mm/yr) are computed for CONUS covering the period of 2003-2017.

State ID,Name	W3RA	MCMC-DA	State ID,Name	W3RA	MCMC-DA
1-West Virginia	-3.69±0.39	**-1.39±0.36**	**25-Ohio**	-1.54±0.28	**0.38±0.15**
2-Florida	-1.01±0.43	**1.47±0.40**	**26-Texas**	-0.11±0.34	**-2.96±0.56**
3-Illinois	0.35±0.24	**1.7±0.44**	**27-Colorado**	-0.13±0.22	**-0.59±0.13**
4-Minnesota	-0.22±0.24	**-1.01±0.30**	**28-South Carolina**	-3.04±0.45	**1.03±0.30**
5-Washington D.C.	-2.83±0.31	**-1.36±0.24**	**29-Oklahoma**	-0.22±0.31	**-2.38±0.41**
6-Rhode Island	-3.42±0.31	**0.09±0.14**	**30-Tennessee**	-1.72±0.47	**-0.42±0.58**
7-Idaho	0.08±0.3	**0.34±0.19**	**31-Wyoming**	0.39±0.22	**1.56±0.20**
8-New Hampshire	-4.30±0.39	**-1.84±0.23**	**33-North Dakota**	-0.18±0.19	**0.22±0.12**
9-North Carolina	-2.65±0.43	**0.13±0.05**	**34-Kentucky**	-2.28±0.39	**-0.73±0.23**
10-Vermont	-3.46±38	**-1.48±0.22**	**38-Maine**	-1.46±0.39	**0.31±0.21**
11-Connecticut	-4.6±0.32	**-0.77±0.16**	**39-New York**	-3.27±0.35	**-0.93±0.21**
12-Delaware	-3.14±0.31	**-1.78±0.31**	**40-Nevada**	-1.03±0.19	**-1.65±0.15**
13-New Mexico	-0.10±0.22	**-2.67±0.33**	**43-Michigan**	0.41±0.25	**0.96±0.28**
14-California	-2.63±0.32	**-4.95±0.44**	**44-Arkansas**	0.02±0.39	**-0.06±0.19**
15-New Jersey	-3.82±0.31	**-0.62±0.30**	**45-Mississippi**	0.60±0.49	**0.26±0.83**
16-Wisconsin	0.45±0.17	**1.86±0.14**	**46-Missouri**	0.34±0.48	**1.08±0.54**
17-Oregon	-0.64±0.34	**-0.63±0.26**	**47-Montana**	0.73±0.22	**1.67±0.18**
18-Nebraska	0.15±0.20	**1.40±0.21**	**48-Kansas**	-0.18±0.23	**-1.26±0.44**
19-Pennsylvania	-3.63±0.35	**-1.37±0.27**	**49-Indiana**	-0.64±0.26	**0.74±0.40**
20-Washington	1.95±0.41	**0.95±0.32**	**51-South Dakota**	0.01±0.2	**0.69±0.22**
21-Louisiana	2.55±0.48	**1.12±0.42**	**52-Massachusetts**	-4.47±0.34	**-1.04±0.25**
22-Georgia	-2.64±0.49	**0.42±0.04**	**53-Virginia**	-2.61±0.40	**-0.63±0.42**
23-Alabama	-1.63±0.54	**-0.83±0.71**	**55-Iowa**	0.66±0.20	**1.51±0.27**
24-Utah	-0.38±0.20	**-0.59±0.22**	**56-Arizona**	-0.18±0.19	**-1.21±0.26**

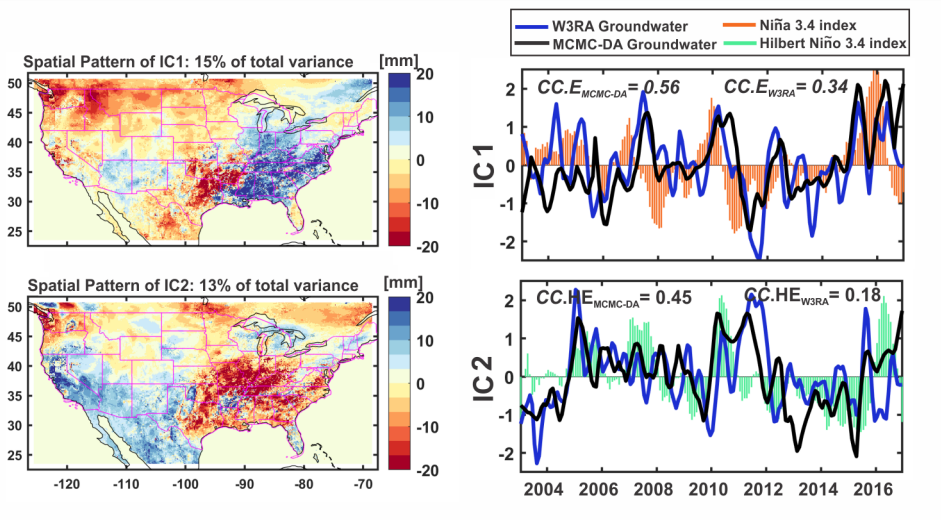

Figure 4: Results of the ICA, which is used to extract the ENSO modes from groundwater storage changes after removing the linear trend and seasonal cycles ($\sim$ 59% of total variance) covering 2003-2017. The spatial anomaly map and its corresponding unit-less temporal evolution on Fig. 4 top represent the first independent mode. The second independent mode is shown on Fig. 4 bottom. For this figure, ICA is applied on groundwater storage changes from MCMC-DA. Then, W3RA estimates are projected onto the spatial components to make a fair comparison. The Niña 3.4 index and its Hilbert transformed time series are shown alongside the IC1 and IC2, respectively. Correlation Coefficient values are shown by 'CC' in this figure, where $CC.E_{\text{MCMC-DA}}$ and $CC.HE_{\text{MCMC-DA}}$ mean Correlation coefficient between ENSO index and temporal pattern of MCMC-DA groundwater storage, and between Hilbert ENSO index and temporal pattern of MCMC-DA groundwater storage respectively. The terms of $CC.E_{\text{W3RA}}$ and $CC.HE_{\text{W3RA}}$ mean Correlation coefficient between ENSO index and temporal pattern of w3RA groundwater, and between Hilbert ENSO index and temporal pattern of W3RA groundwater respectively.

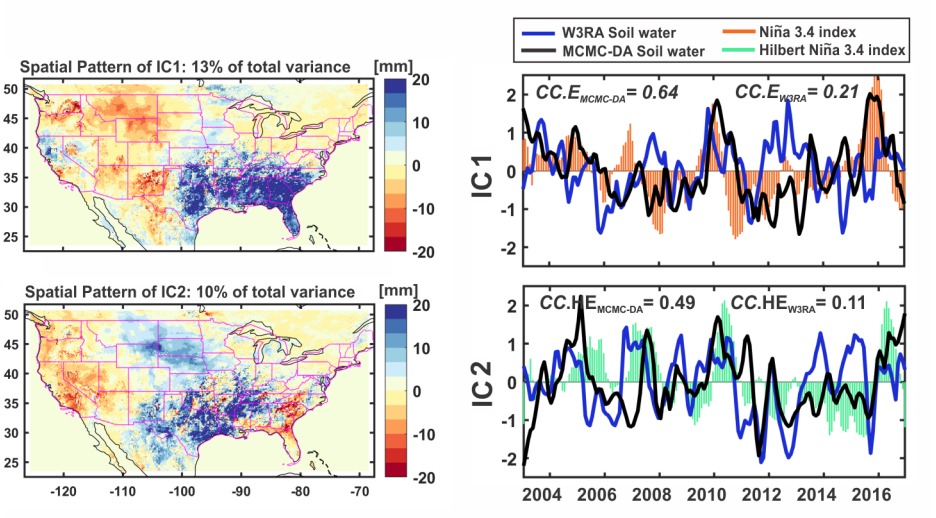

Figure 5: Results of the ICA, which is applied to extract the ENSO modes from MCMC-DA derived soil water storage changes after removing the linear trend and seasonal cycle ($\sim$ 43% of total variance) between 2003-2017. This figure shows the first two independent modes with the spatial and temporal pattern of IC1 on top and those of IC2 on bottom. The spatial patterns correspond to the MCMC-DA. to make a fair comparison, the soil water storage estimate from W3RA are projected onto these spatial components. The Niña 3.4 index and its Hilbert transformed time series are shown alongside the IC1 and IC2, respectively. Correlation Coefficient values are shown by 'CC' in this figure, where $CC.E_{\text{MCMC-DA}}$ and $CC.HE_{\text{MCMC-DA}}$ mean Correlation coefficient between ENSO index and temporal pattern of MCMC-DA soil water storage, and between Hilbert ENSO index and temporal pattern of MCMC-DA soil water storage respectively. The terms of $CC.E_{\text{W3RA}}$ and $CC.HE_{\text{W3RA}}$ mean Correlation coefficient between ENSO index and temporal pattern of w3RA soil water storage, and between Hilbert ENSO index and temporal pattern of W3RA soil water storage respectively.

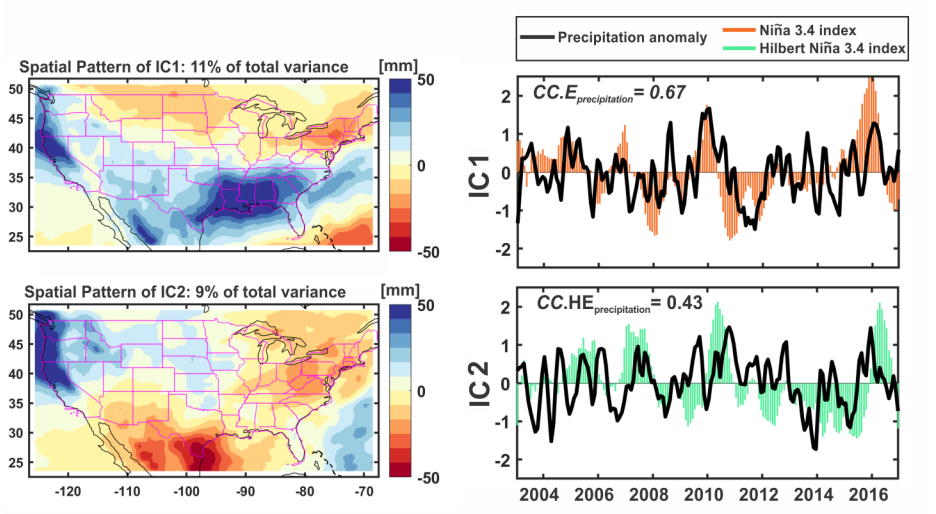

Figure 6: Results of the ICA that is applied to extract the ENSO modes from Precipitation anomalies within the CONUS. The linear trend and seasonal cycles ($\sim$ 53% of total variance) between 2003-2017 are removed from these time series before applying the ICA. This figure shows the first two independent modes, where the spatial and temporal patterns of IC1 are shown on top and those of IC2 on bottom. of the residual signal derived from precipitation anomaly (i.e., corresponded to the ENSO mode), and their relation with Niño 3.4 index and its Hilbert transform. The Niña 3.4 index and its Hilbert transformed time series are shown alongside the IC1 and IC2, respectively, where $CC.E_{\text{precipitation}}$ and $CC.HE_{\text{precipitation}}$ mean Correlation coefficient between ENSO index and temporal pattern of precipitation anomaly, and between Hilbert ENSO index and temporal pattern of precipitation anomaly respectively.

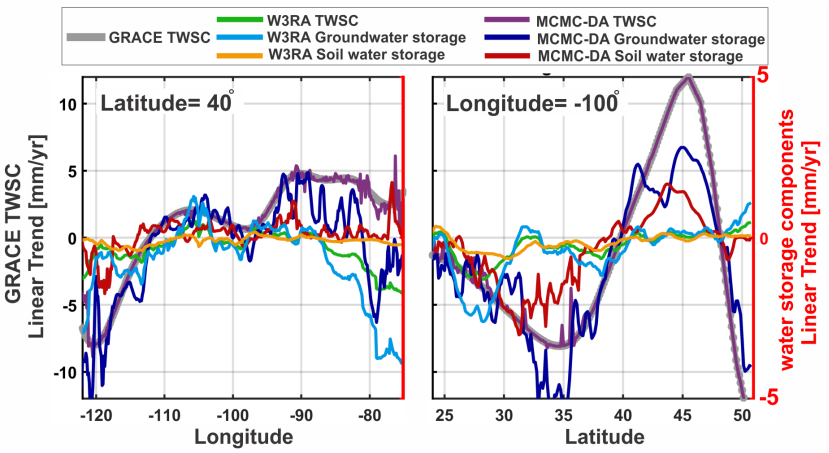

Figure 7: (Left) The latitudinal (the longitude is fixed at $-100°$) and (Right) the longitudinal (the latitude is fixed at $40°$) profiles derived from the linear trends of GRACE TWSC, W3RA TWSC, groundwater and soil water storage, as well as MCMC-DA TWSC, groundwater and soil water storage. In this figure, the left y-axis corresponds to the linear trend of GRACE TWSC, and the right y-axis corresponds to the linear trend of the individual water storage states from the original W3RA and MCMC-DA.

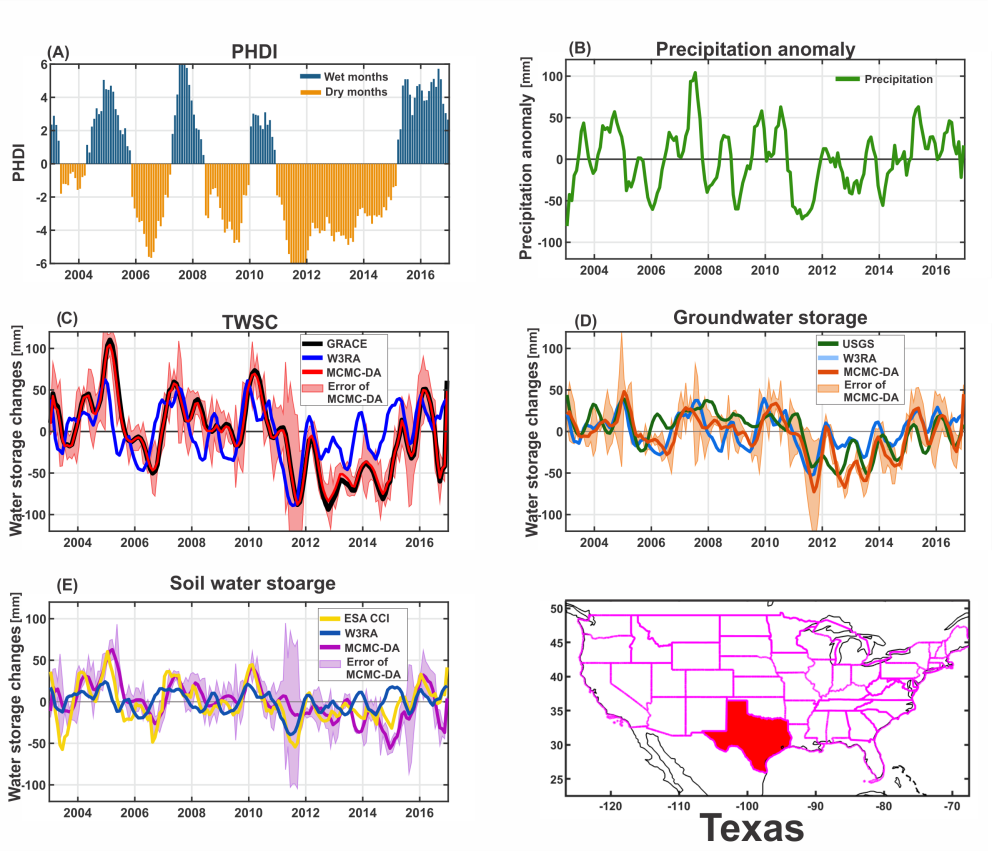

Figure 8: An overview of hydro-climatological changes within Texas, where the spatially averaged time series correspond to (A) the Palmer Hydrological Drought Index (PHDI), (B) precipitation anomalies, (C) TWSC derived from GRACE, W3RA, and MCMC-DA, (D) groundwater storage derived from USGS observations, W3RA, and MCMC-DA, as well as (E) soil water changes derived from ESA CCI products, W3RA, and MCMC-DA.

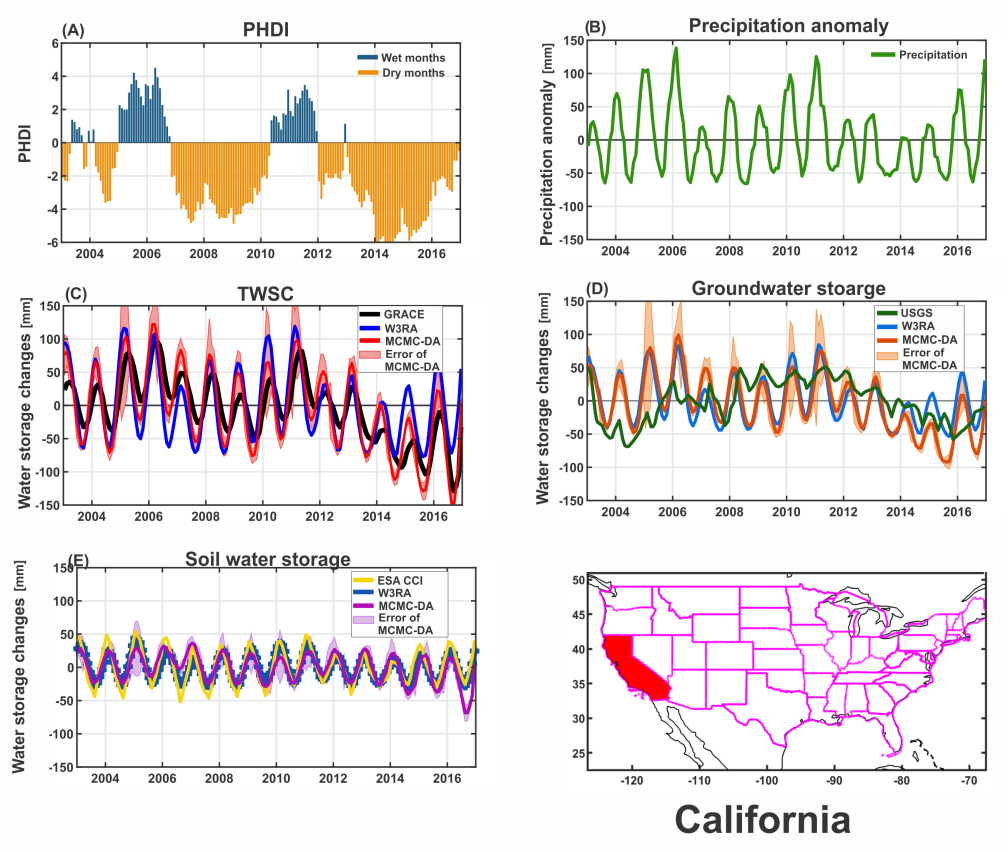

Figure 9: An overview of hydro-climatological changes within California, where the spatially averaged time series correspond to (A) the Palmer Hydrological Drought Index (PHDI), (B) precipitation anomalies, (C) TWSC derived from GRACE, W3RA, and MCMC-DA, (D) groundwater storage derived from USGS observations, W3RA, and MCMC-DA, as well as (E) soil water changes derived from ESA CCI products, W3RA, and MCMC-DA.